Master Thesis

M. Tiemens

Ionization and fragmentation by keV ions and energetic photons of protonated oligonucleotides produced by Electrospray Ionization

The effects of different types of ionising radiation on gas phase oligonucleotides d(GCAT) and d(GTAT) has been investigated by irradiation with keV ions and VUV and soft X-ray photons (15 – 570 eV) using time-of-flight mass spectroscopy. The molecules were brought into the gas phase using Electrospray Ionisation. On all instances, the molecules showed similar dissociation patterns, mostly involving both charged and protonated nucleobase loss and the formation of a specific fragment of 2-deoxy-D-ribose. By also taking into account less pronounced product fragments, information on the weak spots of the molecules could be deduced. Hierarchies for the nucleobase yields were constructed, and two models have been proposed to explain the trends observed. Unlike in experiments performed on single deoxyribose molecules, the readily observed fragments showed that a significant part of these molecules is able to survive irradiation when they are incorporated into larger structures.

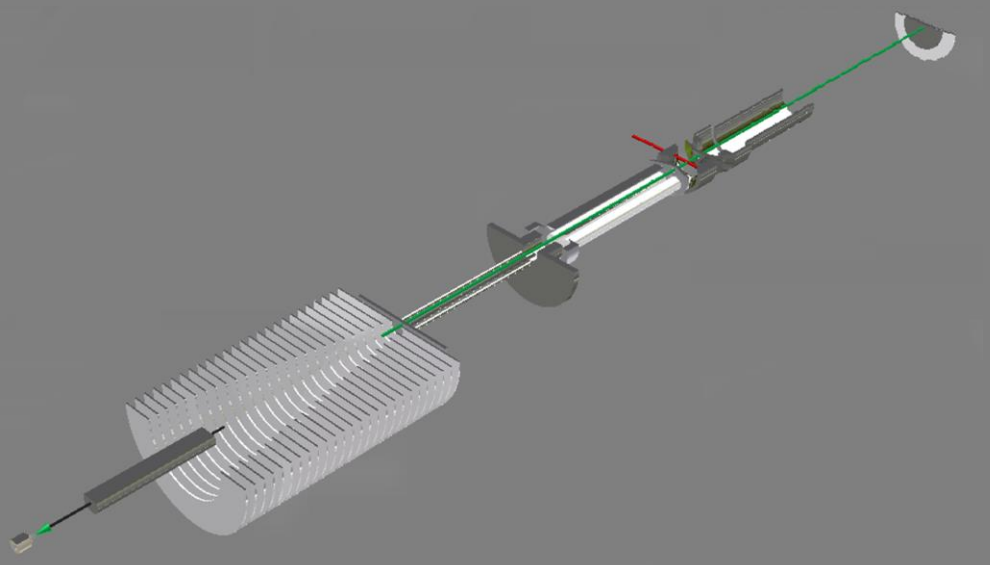

Supervisors: Dr. T. Schlathölter, Prof. Dr. ing. R. Hoekstra
External referee: Dr. S. Hoekstra

university of groningen

KVI

Table of Contents

Chapter I
Introduction

In this section, you can find:

- Motivations for researching radiation damage
- The goal of the experiment
- Information on the biomolecules to be studied
- The path to complex biomolecules

Science is built up of facts, as a house is built of stones; but an accumulation of facts is no more science than a heap of stones a house.
- Jules-Henri Poincare

1.1 Radiation damage

Ever since Marie Curie died of radiation poisoning as a result of her research, scientists have been studying the mechanisms that cause different radiation types to damage living tissue. Most biological effects of ionising radiation were found to originate from direct and indirect DNA damage. The latter is mainly due to interactions with radicals or their complementary electrons formed by radiolysis of the surrounding water. Direct radiation damage can be caused by interactions with ions or photons. In real biological systems, radiation damage is induced by a complex interplay of both types. DNA damage can be repaired by cells to some extent, but in the cases where it can't the cell either dies or mutates. The latter case is most troubling, since it can cause cancer formation.

The current research focuses on direct radiation damage only. It is not clear how the DNA molecules cope with the energy being fed into them when parts of the DNA are excited through interactions with the ionising radiation. Gaining insight into this process is the focal point of this experiment. There are two main motivations for this research. Aerospace and airplane personnel are exposed to increased doses of radiation (mostly photonic), so it may be useful to understand how this damages their DNA. Furthermore, to counteract the tumours, in cancer therapy, the tumours are irradiated with X-ray photons or ions (protons or carbon ions) in order to destroy their cells by inflicting damage to the cell's DNA. Understanding how this works on the molecular level may help to improve the therapy's effectiveness, as well as being interesting from a fundamental point of view. It is on this application that the choice of projectile particle is based; in this study, energetic photons and keV carbon ions are used. Additionally, several experiments using helium ions were carried out to compare different types of ions.

1.2 Starting small

The way any system handles increments in internal energy obviously depends on its size. The DNA molecule is a very large system, and exhibits a great deal of structure on various length scales, which would influence the way it copes with excess energy. The current experiment fits in a series of studies performed by various researchers over the past decades, trying to understand the dynamics from a bottom-up approach, i.e. starting with the building blocks that make up the DNA molecule.

DNA, or Deoxyribose Nucleic Acid, is a biological molecule (or biomolecule for short) that has encoded in its structure specific sequences to create proteins of various sorts. The parts of the DNA that make up the genetic code are the nucleic acid bases (or nucleobases for short). There are exactly four different types of nucleobases in DNA, namely guanine (G), cytosine (C), adenine (A) and thymine (T), the structures of which are shown in figure 1.1.

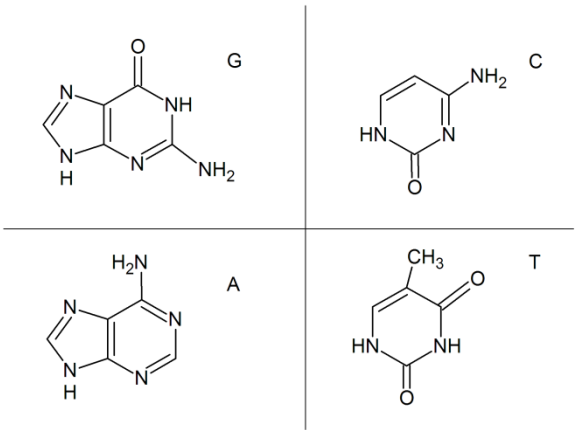

Figure 1.1: The four DNA nucleobases guanine (G), cytosine (C), adenine (A) and thymine (T).

It is evident that damage to the nucleobases disrupts the genetic code and can lead to various mutations. Radiation damage to the nucleobases by the types mentioned in section 1.1 has been studied by various researchers. Both keV and high-charge ions (protons [1], carbon ions [2], oxygen ions [2], argon ions [3] and xenon ions [4]) were observed to have a devastating effect on the nucleobases, as they nearly completely disintegrate upon irradiation. With very highly charged, low velocity ions, the bases sometimes even break apart into atomic ions [4].

Photons will only form ionised product fragments when their energy exceeds 12 – 14 eV, but will still induce damage below this threshold [5, 6]. Electron attachment studies found dehydrogenation, i.e. proton emission, to be an important fragmentation channel for adenine, thymine and cytosine. Abdoul-Carime *et al*. [7] proposed that the hydrogen radical that is released can induce further damage to the DNA, although in larger structures, cleavage of the bond linking the bases to the DNA backbone would be more likely. Experiments performed by de Vries *et al*. [4] found dehydrogenation to be the first step in the fragmentation process. However, for guanine, proton emission was observed to only modestly contribute [8, 9]. In that case, the molecule mostly dissociates by loss of cyano structures. Incidentally, this was also found to be a major channel for thymine (with an additional oxygen atom attached) [6] as well as adenine [3, 6] when employing other radiation types.

Scaling up the system, Schlathölter *et al*. looked into clusters of nucleobases [2]. Already in small clusters, dissociation channels opened up that were found to be closed in the isolated molecules. They also found that the most favourable arrangement for these clusters was a planar geometry, formed by hydrogen bonds, which incidentally also is how the paired bases are bound into the DNA double strand. Clearly then, the need to expand the studies to even larger systems is evident.

1.3 Sugar forms the backbone of life

In supplement to the nucleobase studies, various experiments have been dedicated to the sugar structures that are part of the backbone and incorporate the nucleobases into the larger structure. The systematic name for the sugar structure is 2-deoxy-D-ribose[1]; for its structure, see figure 3.4. Under all radiation types mentioned in section 1.1, the 2-deoxy-D-ribose molecule was found to nearly completely disintegrate [10 – 13]. When using low energy electrons, the structure was found to lose the equivalent of 2 water molecules [10].

To quantify the fragility of this molecule, Ptasinska *et al*. [10] noted that, when using high energy electrons, the relative amount of fragment ions compared to that of the parent cation is about an order of magnitude larger than it is in the case of the nucleobases. In their experiments

[1] All occurrences of 'deoxyribose' or 'sugar' throughout the discussion will refer to 2-deoxy-D-ribose.

with protons and helium ions, Alvarado *et al*. [12] found the distribution of fragments to be mostly statistical.

1.4 From building blocks to complex biomolecules

The next step is to look at more complex systems comprised of the aforementioned building blocks. The sugar moieties and nucleobases link together to form the (single strand) DNA secondary structure, as shown in figure 1.2. A small piece of single stranded DNA or RNA is called an oligonucleotide. The name stems from *oligo*, meaning small in Latin, and *nucleotide*, which is a specific part of the DNA structure (see section 3.5.3). Liu *et al*. [14] looked into the stability of one of the nucleotides containing adenine by means of high energy/single collision Collision-Induced Dissociation (CID). They found that the nucleotide mostly fell apart into the nucleobase and complementary fragment or by excision of the phosphate group.

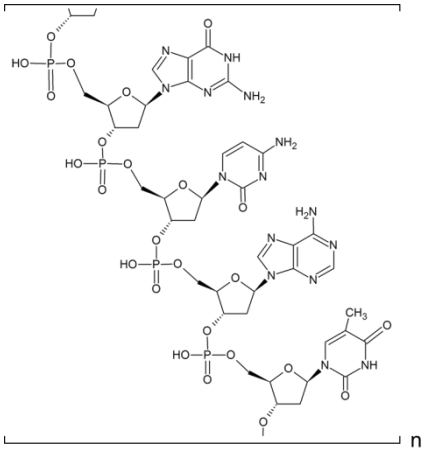

Figure 1.2: Example section of the DNA secondary structure.

Moving on to even larger structures, in the study at hand, oligonucleotides containing four bases were used. These are often also referred to as tetramers. Similarly, those containing three or two nucleobases are called trimers and dimers, respectively. As will be explored in chapter V, both the nucleobases and the sugar moieties are largely able to survive irradiation intact, when they are incorporated in these larger biomolecules. This was also found to be the case for trimers [15] and dimers [16]. More information on the oligonucleotides used in these experiments can be found in section 3.3.

Chapter II

Theory

In this chapter, you can find:

- The classical over-the-barrier model
- Ionisation pathways for ionic and photonic irradiation

If all of mathematics disappeared, physics would be set back by exactly one week.
- Richard P. Feynman

2.1 Ionisation: the classical over-the-barrier model

Due to the relatively low target molecule densities and ion fluxes, there will likely be few direct collisions between ions and target molecules. This means that electron capture will be the dominant ionisation path for the experiment at hand. The classical over-the-barrier model provides a decent description for this process. The basic concept is the following. As an ion approaches a molecule, the overlap of the superposition of their potential energy wells starts to increase. When the ion is close enough, an electron from the molecule can make the transition to a (high-energy) state in the projectile ion (see figure 2.1). In doing this, it transits the potential barrier between the ion and the target molecule, hence the name of the model.

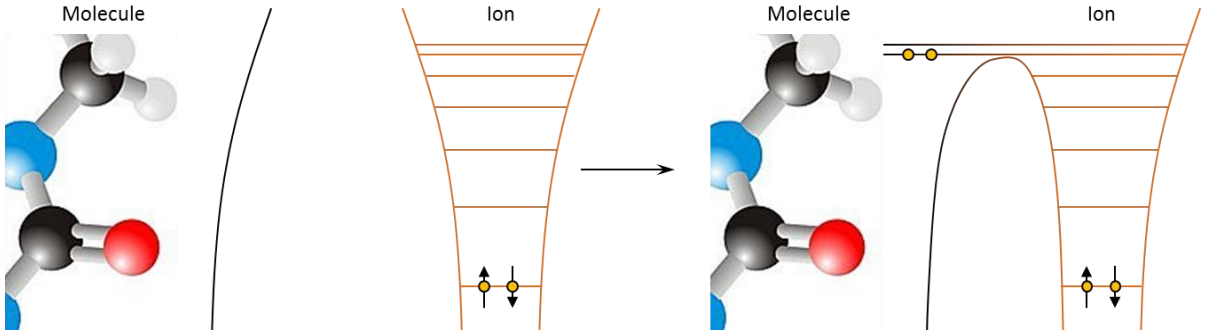

Figure 2.1: As the ion approaches the molecule, the overlap between potentials increases.

2.2 Ionisation pathways

Having introduced briefly the classical over-the-barrier model, we can now look at some of the different pathways through which ionisation of the target molecule might occur. The transfer of the electron between molecule and ion is called Quasi-Resonant Neutralisation, and is an example of Direct Ionisation of the target molecule (see figure 2.2). In this case, the

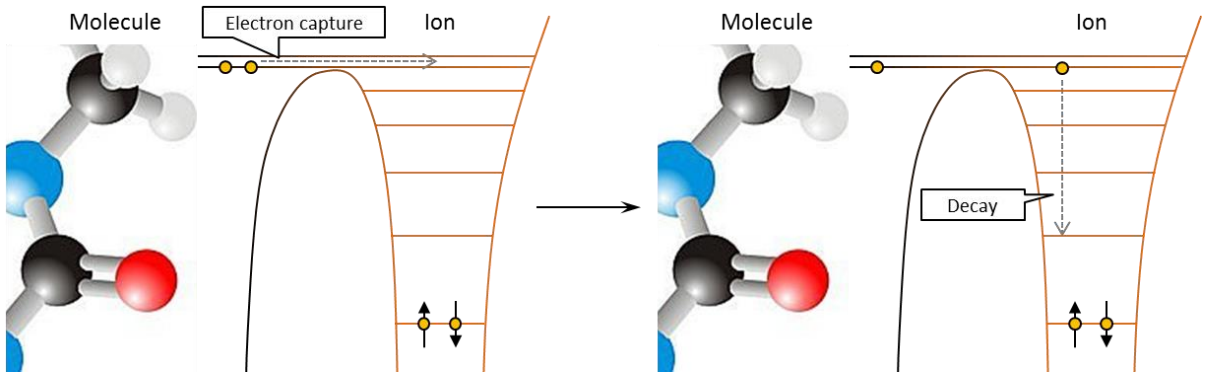

Figure 2.2: When the barrier is low enough, the ion can capture an electron from the molecule.

ionisation occurs through electron capture by the ion. With high charge state ions, multiple electron capture becomes feasible. Note that the term 'Neutralisation' applies to the ion, which is the party that is being neutralised by the electron transfer.

In the case of photonic irradiation, the classical over-the-barrier model obviously no longer applies. Now, the photoelectric effect is responsible for the ionisation of the molecule (see figure 2.3). The absorption of a photon can provide enough energy for Direct Ionisation or put an electron in an excited state. In case the photon ionises one of the electrons from a core shell (as is the case with e.g. X-ray photons), the hole that is left by the ionised electron will be filled by one from a higher energy level. The energy that is released when this transfer occurs can then be absorbed by another electron and excite it to the vacuum state (figure 2.4). This is called Auger de-excitation.

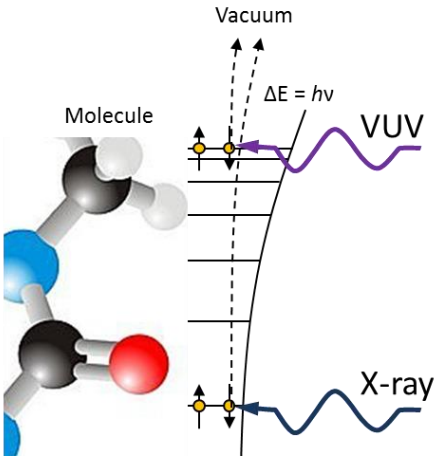

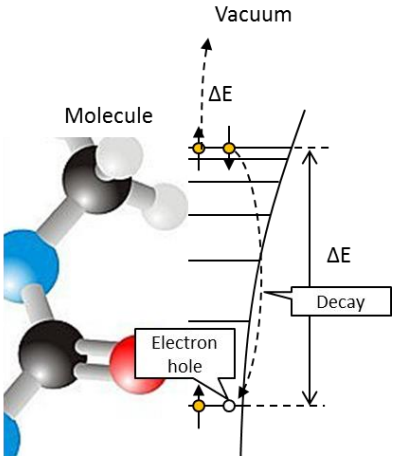

Figure 2.3 (left): Photoabsorption can excite electrons to the vacuum state.

Figure 2.4 (right): Decay of one the electrons in a higher energy level can induce Auger de-excitation.

Following ionisation, charge is redistributed throughout the molecule to lower its total energy. Fragmentation occurs when the redistribution of the electrons excites vibrational states by creating phonons in the molecule. The destructive effect of the phonons was shown to be enhanced further when the vibrational excitations do not completely relax between electron transits and so induce "pumping" of higher vibrational modes of the molecule [17].

Most of the aforementioned processes may also apply to the fragments of the parent molecule. When the fission of the parent molecule doesn't dissipate all of the excess energy, Auger de-excitation processes can still occur, even without the presence of the projectile ion or photon. This may create more highly charged fragments, or induce further fragmentation.

Chapter III

Methods

In this chapter, you can find:

- An introduction to Electrospray Ionisation
- Details of sample compositions
- Information concerning the oligonucleotides used
- How to get information from the recorded signal
- An introduction to the terminology used in the text

To see that which cannot be seen, you must see without looking.
- Anonymous

3.1 Electrospray Ionisation [18]

The most straightforward approach to study the effects of direct radiation damage only is by means of gas phase studies. The DNA building blocks mentioned in the introduction can be put in the gas phase simply by sublimation from the solid phase. Unfortunately, this won't work for the more complex biomolecules such as oligonucleotides, as they already decompose thermally on very moderate heating. To study these molecules in the gas phase, then, requires more gentle techniques. Examples of such techniques include laser desorption and electrospray ionisation. The latter has been chosen for use in the experiment at hand, and shall now be explained in some more detail.

First, the desired molecule needs to be dissolved in a solvent that evaporates rather easily, e.g. water or methanol, together with an acid or basic solution. The reason for adding an acid or base is to add or remove protons from the target molecule, respectively, in order to add charge to the molecule. After this treatment, the molecule is protonated or deprotonated. Next, the sample is pumped through a needle which is set at high voltage (in the order of 5 kV). The potential difference between the needle and the capillary, a narrow tube that forms the entrance to the setup, causes the flow of solvated molecules to form a cone configuration, the so-called Taylor cone. At the end of the cone, droplets with dissolved charged molecules form, that accelerate towards the capillary due to the potential difference with the capillary. During flight, the solvent starts to evaporate. At some point, the charge density in the droplet becomes too large for the surface tension to keep the droplet together (the so-called Rayleigh limit), and the droplet fissions. This is termed a Coulomb explosion. The process of evaporation followed by Coulomb explosion is then repeated until there are only gas phase molecules left.

3.2 A bit of chemistry: Sample compositions

The previous section mentioned the special mixture that is needed to make the electrospray process work. A base or acid is added to the sample to force the formation of a charged molecule. This has the additional advantage that the charged molecules can easily be guided and trapped into the setup. The current setup is optimized for the positive mode, i.e. for positively charged oligonucleotides. Therefore, an acid is added to the sample mixture. The following chemicals and ratios where used: a 40 μM sample of the oligonucleotides was composed of 80% methanol (HPLC Chromasolv, Sigma Aldrich), 20% water (HPLC, Fluka) and 0.5% formic acid (HPLC, Fluka).

3.3 Employing Oligonucleotides

For the experiments described in this work, the oligodeoxynucleotides d(GCAT) (see figure 3.1) and d(GTAT) were used. The addition of "d" in front of the name indicates that the molecules are *deoxy*nucleotides. This has to do with the structure of the sugar moiety, i.e. the five-membered rings in the left hand side of figure 3.1 (also shown in figure 3.4). In the case of deoxyribose, the 2' carbon atom (see figure 3.4) has a hydrogen atom attached, and in the case of ribose, there is a hydroxyl group attached at this position. This feature distinguishes DNA (having deoxyribose) from RNA (which has ribose). The letters G, C, A and T label the four DNA nucleic acid bases (nucleobases for short) guanine, cytosine, adenine and thymine, respectively. In 'real' DNA, the nucleobases pair up to form a double strand. Hence, in this experiment, a piece of single-stranded DNA is used, containing all four DNA nucleobases.

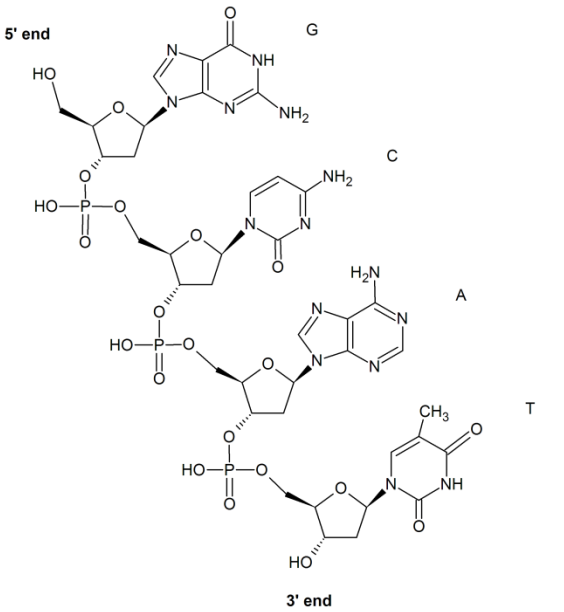

Figure 3.1: Structure of the oligonucleotide d(GCAT). The letters G, C, A and T label the respective nucleobases.

Both employed molecules have been purchased from DNA Technology, situated in Risskov, Denmark, and were used without further processing. The stock solutions were diluted from 1.2 mM to 40 μM using HPLC water to make it easier to prepare samples from them, but even with the diluted solutions, typical amounts laid in the low μL range. With the solvent and acid ratios chosen (see section 3.2), the typical degree of protonation for the oligonucleotides was two, i.e. double protonation. The settings in the experimental setup (see section 4.1) have been optimized accordingly to select, guide and trap the double protonated molecules.

3.4 Extracting the Signal from the Recorded Spectra

Despite the low background pressure and a liquid nitrogen cryo-trap close to the RF trap (see section 4.1), ionised background molecules might still contribute to the mass spectra. To counter this, the mass spectra are recorded in a three-cycle according to the timing settings shown in figure 3.2. First, the target molecules are loaded into the RF trap. During the loading process, a helium buffer gas pulse is applied to

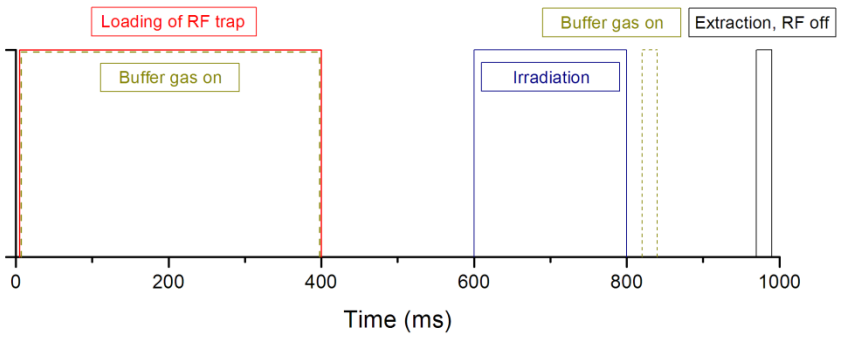

Figure 3.2: Typical timing settings for the three-cycle (see text).

"cool" the molecules (see also section 4.1). Secondly, the trap content is irradiated, directly after which the resulting fragments are cooled using a second buffer gas pulse to increase the mass resolution. Finally, the RF trap is switched off and its contents are extracted. A typical spectrum for each of the three recordings is displayed in figure 3.3. In the first recording, labelled "Loading only", the photon or ion beam is blocked, so the trap content is not irradiated. This spectrum is recorded as a reference for the final signal. The second recording features all the stages in the timing settings. This yields the so-called inclusive scan. During the third and final recording, labelled "Extraction only", the molecular beam is blocked, so that this yields the background originating from ionisation of residual molecules. Finally, the spectra from the first and third recording are subtracted from the inclusive scan, to obtain the spectrum that shows the net production of fragments.

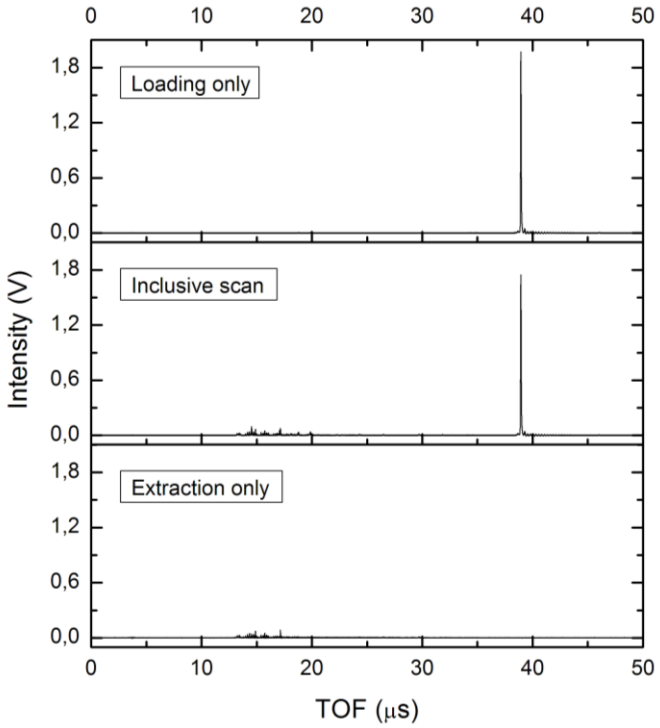

Figure 3.3: Typical spectra for the three-cycle.

In order to gather sufficient statistics on the data, for each experiment, this three-cycle (also referred to as an acquisition) is repeated many times and the final signal is calculated by averaging over all acquisitions. To save time, each new acquisition is added to the existing calculated signal by taking the weighted average of the two, which then becomes the new signal. It can be shown that about 1000 of such acquisitions are required to ensure sufficient statistics for the final spectrum.

3.5 Extracting the physics from the signal

3.5.1 Noise reduction

The signal obtained in the previous section shows a high background and shows the intensity as a function of the flight time, where mass-over-charge (m/z) dependency is desired. The signal needs to be corrected for artefacts due to the 1 GHz sampling frequency as well. The latter is achieved by applying an appropriate band-block filter in the FFT of the signal. The signal is then transformed back and the noise is reduced by adjacent averaging of 13 points.

In general, the data acquisition could not be run long enough to acquire the required average of 1000 acquisitions. The experiments needed to be stopped after a certain number of acquisitions, the settings adjusted to restore the signal from the molecular beam and then the data acquisition would be resumed, but then with a new set of acquisitions. To find the final signal, the information from these experiments needs to be combined in an appropriate way. It

is not hard to see that the more acquisitions a given experiment has, the more statistics the corresponding signal contains. It therefore makes sense to average the signals from the different experiments by weighing each signal by its corresponding number of acquisitions. This way, the final signal was obtained.

3.5.2 The heavier you are, the slower you move – calibrating the mass spectrum

The mass calibration is achieved in the following manner. By equating the kinetic and potential energy of an ion, it can be shown that the following relation holds between the flight time and the m/z ratio (in a field-free region without acceleration):

$$t = \frac{d}{\sqrt{2U}}\sqrt{\frac{m}{z}} + C, \qquad \text{(Eq. 3.1)}$$

where t denotes the flight time, d the distance travelled, U the acceleration potential, m and z the mass and charge of the particle, respectively and C some constant. Some of the parameters in Eq. 3.1 are difficult to obtain, hindering the calculation. Rewriting Eq. 3.1 as

$$t = B\sqrt{\frac{m}{z}} + C \qquad \text{(Eq. 3.2)}$$

enables a different approach. By guessing for some of the peaks in the spectrum to which fragments they correspond, a linear fit can be made through the resulting set of points from the $(\sqrt{(m/z)}, t)$ plot. This way, the parameters B and C can be obtained, fixing the mass calibration.

In order to be able to compare the mass spectra, they must be normalized. In this experiment, the normalization was chosen in such a way that the area of the largest peak (the negative peak corresponding to the loss of the parent molecule, see figure 5.1) is set to one. This way, when fragment yields are calculated, this will be with respect to the yield for the loss of the parent molecule, which always equals one. For a resulting spectrum, see for instance figure 5.1.

3.5.3 Terminology and jargon

Introducing some notation: the addition of +nH to a fragment name denotes a n-fold protonated fragment. The location of the bonds being broken is often referred to by a number, shown in the deoxyribose molecule in figure 3.4. In figure 3.1, the 5' end attribution can be seen to come from the fact that the hydroxyl group at this end is attached to the 5th carbon atom of the deoxyribose moiety. Similarly, the hydroxyl group at the 3' end is attached to the 3rd carbon atom of the moiety. As can be seen in figure 3.1, the deoxyribose moiety is fully incorporated into a larger structure, with bonds at three sites. In the discussion in chapter 5, this group can be seen to not show up in the form shown in figure 3.4, but a 'stripped down' version with cleavages at various sites is observed. Nevertheless, the text will continue to refer to that fragment as the deoxyribose or sugar moiety, even though strictly speaking it is only a fragment of this molecule. Figure 3.5 shows some additional jargon, concerning product ion structures, that is used in the fragmentation discussion in chapter 5.

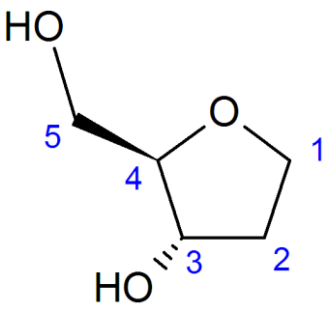

Figure 3.4: Numbering jargon employed in the discussion.

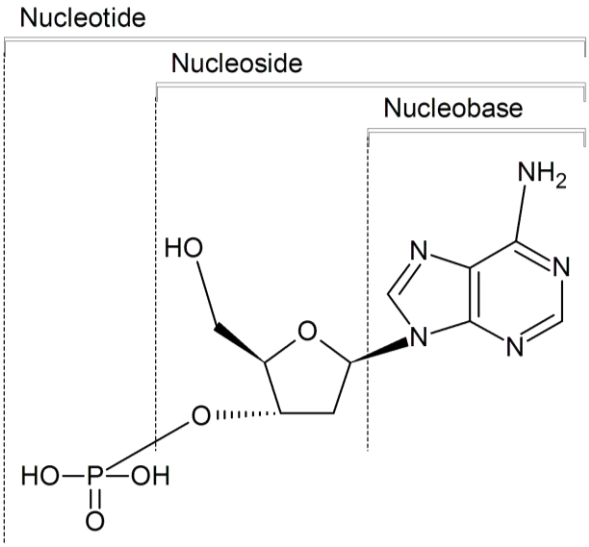

Figure 3.5: Widely used structural jargon in articles on DNA, RNA, oligonucleotides and their constituents. The nucleosides corresponding to the four nucleobases are called deoxyguanosine (dG), deoxycytidine (dC), deoxyadenosine (dA) and thymidine (dT).

Chapter IV
Experimental setup

In this chapter, you can find:

- An overview of the experimental setup
- Information about the ECRIS facility at the KVI
- Information about the MAX-lab facility in Lund
- Information about the BESSY II facility at the HZB

Things should be made as simple as possible, but not any simpler.
- Albert Einstein

4.1 The Paultje Setup

The experiments were performed using a home built experimental setup called "Paultje". The name is based on the Paul trap, which is a key component of the setup. Figure 4.1 shows a schematic view of the setup, the details of which will be highlighted in the list below.

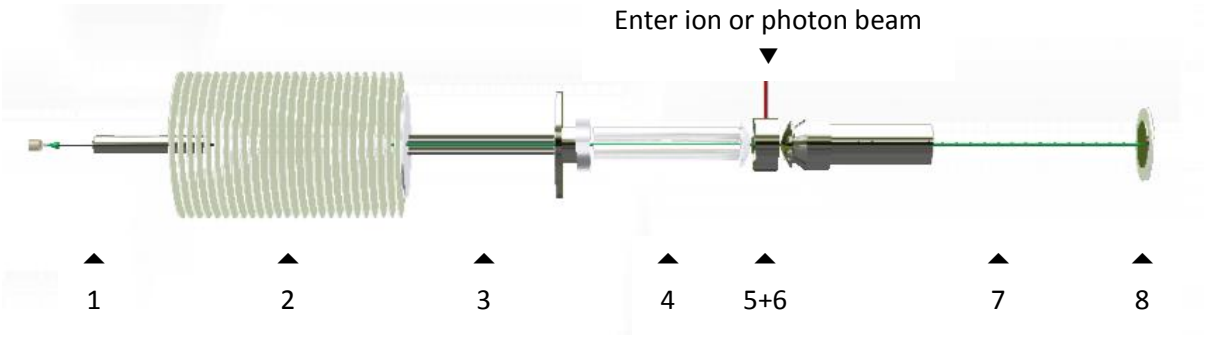

Figure 4.1: Schematic representation (top view) of the Paultje experimental setup.

1. Electrospray and capillary. The molecules are brought into the setup using a method called Electrospray Ionisation (ESI, see section 3.1 for more information). The electrospray device is home-build. The samples are pumped through an insulated tube at a typical rate of 0.2 mL/h. The tuneable high-voltage bias of the needle was set to about 4 kV and the device was operated under atmospheric conditions. Through 3 jackscrews in the insulated holder, the needle position could be adjusted in all three Cartesian coordinates. The molecules enter the setup through a narrow capillary tube with an inner diameter of 0.1 mm, which was closed using a stopper when no experiment was running. To help prevent water cluttering up the capillary and increase the solvent evaporation rate, the capillary was heated to about 100° C.
2. Ion funnel. Upon leaving the capillary, the molecules pass through a radiofrequency (RF) ion funnel in the first vacuum chamber, consisting of 26 0.5 mm thick interconnected ring electrodes with inner diameters decreasing linearly from 38.1 mm for the first 10 electrodes (made of copper) to 7.9 mm over the other 16 electrodes (made of stainless steel) towards the 1 mm diaphragm located at the exit. The array is based on the design of Julian *et al*. [19], and is generally operated at a frequency of 1040 kHz with a RMS voltage of 85 V. These parameters can be tuned to optimize the signal from the electrospray device. A superimposed DC electric field ensures a net force towards the exit diaphragm. The ion funnel was designed to compress the phase space of the molecules and filter out some of the background molecules that drift along with the desired particles. During operation, the open capillary would expose the ion funnel to almost atmospheric pressure. To help maintain a low pressure in this region, a roots pump (Pfeiffer Vacuum, type: WKP 250) was activated whenever the capillary was opened. This maintained a base pressure of 0.5 mbar during operation. When the capillary is closed, the pressure drops to $1 \cdot 10^{-3}$ mbar.
3. First quadrupole. To compress the phase space further, the cations are guided through a RF only quadrupole ion guide in the second vacuum chamber. The pressure in this part

of the setup laid around $1 \cdot 10^{-4}$ mbar with the capillary opened, and $1 \cdot 10^{-6}$ mbar with the capillary closed. During data acquisition, pulsing of the cation beam (section 3.4) was achieved by biasing the entrance diaphragm (which is also the ion funnel's exit diaphragm) to 200 V. This prevented the cations from entering the ion guide.

4. Quadrupole mass filter. At this point, the cation beam still contains a lot of different particles. To be able to select a specific mass-over-charge (m/z) state, the beam crosses through a quadrupole mass filter. An oscillating RF electric field over each pair of rods allows for a mass-selective transition of particles through the device. Which m/z states are able to transit the mass filter can be calculated by solving the Mathieu equations [20]. As with the ion funnel, a superimposed DC electric field ensures a net flow towards the mass filter's exit.
5. 3D RF or 'Paul' trap. Having selected the particle with the desired m/z state, it is important to note that the ESI method yields relatively low-intensity cation beams. In order to acquire sufficient target densities for experiments, the cations are trapped and stored in a three dimensional RF ion trap. For the purpose of these experiments, the type of ion trap used was a so-called Paul trap, named after Wolfgang Paul, who developed the foundation for this type of ion traps and received the Nobel Prize in Physics in 1989 for his work. The Paul trap consists of a pair of hyperbolic electrodes and a hyperbolic ring electrode (see figure 4.1). The trapping region can be obtained from the equations of motion by solving the Mathieu equations. Particles were focused into the trap through an Einzel lens. To decrease the kinetic energy of the cations, a helium buffer gas pulse is applied. This is needed to trap the molecules, since they would be able to overcome the potential barrier created by the ion trap with ease when their kinetic energy is too high. The trap content is exposed to an ion or photon beam, after which cationic dissociation product fragments are formed and extracted (see also section 3.4). The base pressure in the fourth vacuum chamber was about $1 \cdot 10^{-8}$ mbar, which increased to $1 \cdot 10^{-4}$ mbar during He pulsing.
6. Cryo-trap (not shown in figure 4.1). To reduce the background, a liquid nitrogen cryo-trap is placed directly above the Paul trap.
7. TOF tube. Extraction of the trap content was achieved using a pulsed voltage, which accelerated the biomolecular dications and accompanying dissociation products into a linear, biased time-of-flight (TOF) tube. The bias high voltage of about -3 kV ensured a net drift towards the detector. The TOF tube has a length of 82 cm, enabling a resolution of $m / \Delta m = 200$. Base pressure in the TOF tube was around $1 \cdot 10^{-9}$ mbar, running up to $1 \cdot 10^{-6}$ mbar when the He pulses were applied.
8. Detector. The detector is a silhouette-type detector with two micro channel plates (MCP) in chevron configuration (50 mm diameter) and an anode, which provides the signal for read-out. The front plate of the MCP's was set to a voltage of -5 kV, such that the voltage drop between the plates was 1700 V, with the anode kept grounded. The anode was connected to a 1 GHz digitizer residing in a PC for data acquisition (see section 3.4). Data was recorded in custom software designed using Labview 2009.

4.2 ECRIS

The ion-induced fragmentation studies were performed using an ion beam, extracted from the Electron Cyclotron Resonance Ion Source (ECRIS) located at the ZernikeLEIF facility at the Kernfysisch Versneller Instituut (KVI) in Groningen, The Netherlands. In the source, a magnetic bottle is created, which is formed by superimposing a longitudinal field supplied by two coils and a radial field generated by a permanent hexapole magnet. When inside the magnetic bottle, electrons gyrate at the cyclotron frequency $\omega_c = 2\pi eB / m_e$ due to the Lorentz force. When a 14 GHz radiofrequency field is applied at the same frequency as ω_c, the electrons are resonantly accelerated, ionizing gas molecules of the desired species through (multiple) collisions as they traverse the magnetic bottle. This method creates a variety of m/z states, which are extracted through an extraction lens. To select the desired m/z ratio, a 110° analysing magnet is employed directly behind the exit of the ECR source. Tuning the magnetic induction of the magnet allows for the selection of a specific state by means of the m/z –dependent Lorentz force experienced by the ions. For the purposes of the experiment at hand, the ECR source was tuned to produce ion beams of He^{n+} (n = 1, 2) and C^{n+} (n = 2 – 5) in the energy range of 16 – 60 keV/u. The beams produced are guided to the experiments through a series of quadrupole magnets and a 45° deflection magnet. To determine the ion current at the setup, a Faraday cup was placed behind the Paul trap. Exposure time was controlled by means of an electrostatic deflection field located inside the ion beamline.

4.3 MAX-II

The experiments in which the photosensitivity was studied were performed at two synchrotron facilities, at two energy ranges. In general, a synchrotron is a type of cyclic particle accelerator in which the guidance magnetic and electric fields are time-dependent [21]. The fields are synchronized (hence the name) to the particle beam traversing the synchrotron to circulate and accelerate the particles. The facilities described in this and the following section are so-called synchrotron light sources, which consist of an electron storage ring containing undulators. A storage ring is a special type of synchrotron in which the kinetic energy of the particles in the accelerator is kept constant. An undulator is a periodic arrangement of dipole magnets in which each subsequent magnet has its polarity reversed with respect to its neighbours. The continuous flipping of the polarity of the magnetic fields causes electrons traversing the array to oscillate and consequently radiate. This principle is also used in free electron lasers (FEL's), and generally yields very high luminosities. The beamlines are located in line of the undulators.

First up, the 3rd generation synchrotron facility MAX-II located at MAX-lab in Lund, Sweden, was used to produce photons in the high energy vacuum ultraviolet (VUV) photon energy range (40 eV – 100 eV) and the soft X-ray regime (150 eV – 570 eV), probing both valence and core shell electron ionization of carbon, nitrogen and oxygen. The MAX-II storage ring has a circumference of about 90 m and electrons are accelerated to energies up to 1.5 GeV [22]. The experiments were carried out at the beamline i411. The beamline's undulator consists of 43 dipole magnets with a length of 59 mm each. A modified SX-700 monochromator equipped with a 1220 lines/mm grating delivered a flux typically exceeding 10^{12} photons/s. The resolution lay between 500 meV and 1000 meV, depending on the photon energy chosen. The photon flux was determined using a SXUV-type silicon p-n junction photodiode (IRD, Newbury Park, USA) and

the exposure time was always controlled using a mechanical shutter with a 14 mm aperture (Uniblitz, Rochester, USA).

4.4 BESSY II

The setup had also been interfaced with the 3rd generation electron storage ring facility BESSY II (figure 4.2), located at the Helmholtz-Zentrum Berlin in Berlin, Germany. The facility's synchrotron has a circumference of about 240 m and electrons are accelerated to energies up to 1.7 GeV [23]. The photons, having energies in the range of 15 – 24 eV (low energy VUV), were produced in the quasi-periodic undulator U125/2. The array has 32 dipole magnets with a periodic separation of 125 mm. To prevent transmission of higher harmonics through the monochromator, the undulator has dislocations in the periodic pattern, making it quasi-periodic. Photon energy tuning was achieved using a 10 m focal length normal incidence monochromator. For a maximum photon flux of 10^{13} photons/s, a 300 lines/mm grating was employed. The energy resolution achieved was about 250 meV.

Figure 4.2: The third generation synchrotron facility BESSY II in Berlin, Germany.

Chapter V

Results

In this chapter, you can find:

- General features of the recorded mass spectra
- Comparison of ionic and photonic irradiation types
- The effect of replacing cytosine in d(GCAT) with thymine
- What can be learned from these results

In theory, there is no difference between theory and practice. But, in practice, there is.
- Jan L. A. van de Snepscheut

5.1 Generic features of the mass spectra

The spectrum obtained in section 3.5 has a number of features that are common to nearly all recorded mass spectra. Figure 5.1a shows a typical calibrated mass spectrum for the molecule d(GCAT). The largest peak in the spectrum is negative, and corresponds to the loss of the parent d(GCAT) molecule. In the low mass-over-charge range, five peaks can be seen standing out. As shown in the zoomed plot in figure 5.1b, these peaks originate from the deoxyribose or sugar moiety (s) in the oligonucleotide and the four nucleobases: cytosine (C), thymine (T), adenine (A) and guanine (G). These peak assignments follow the ones of previous experiments [16, 24]. The sixth major peak at m/z = 392 belongs to the ionised parent molecule. A closer inspection of the peaks corresponding to the nucleobases reveals that they are in fact double peaks (see also

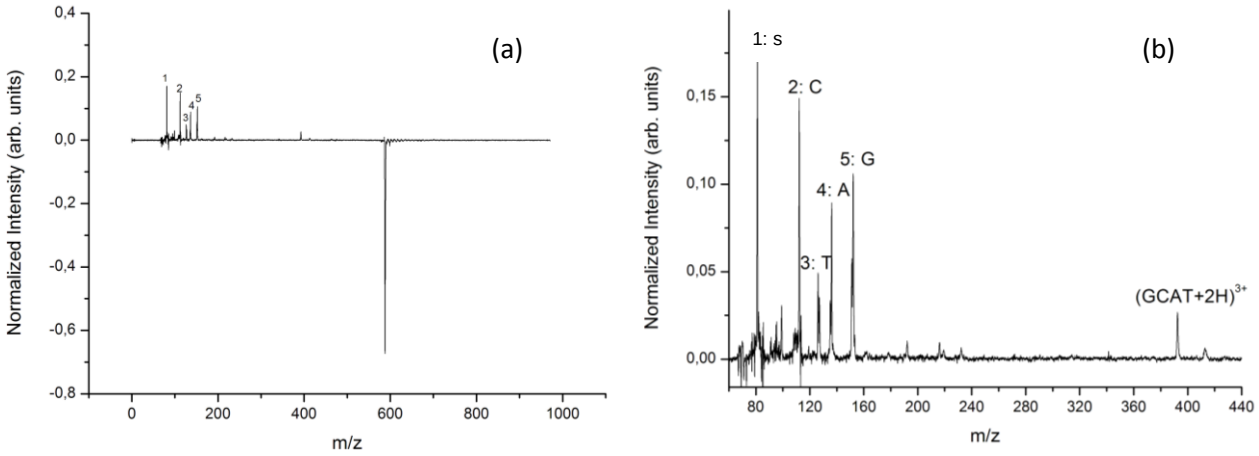

Figure 5.1a and b: Generic examples of calibrated mass spectra.

figure 5.2). The twin peaks consist of the protonated nucleobase and the non-protonated, charged nucleobase. In some spectra that did not use a second buffer gas pulse to cool the fragments, it was not always possible to properly resolve the two peaks. For most spectra, the ratio between these two overlapping peaks is not identical, as will be explored in more detail in section 5.2. A number of minor fragments (in terms of fragment product yields) can also be identified in the spectra. Section 5.4 will look into these fragments, which are also common to most spectra, albeit with different yields.

5.2 Ionic irradiation versus photonic irradiation

The experiment was performed with different radiation types: helium and carbon ions, VUV photons and soft X-rays. This discussion will start with ionic irradiation and then compare the results with the ones obtained from using photonic irradiation. In order not to clutter up the pages with endless plots of mass spectra, only a small set of typical spectra is shown. For a complete set of recorded mass spectra, see Appendix A.

5.2.1 Ionic irradiation

Figure 5.2a shows (a portion of) the mass spectrum resulting from C^{4+} irradiating a d(GCAT) target. Comparing with figure 5.2b, showing the same target being irradiated by He^{2+}, the low

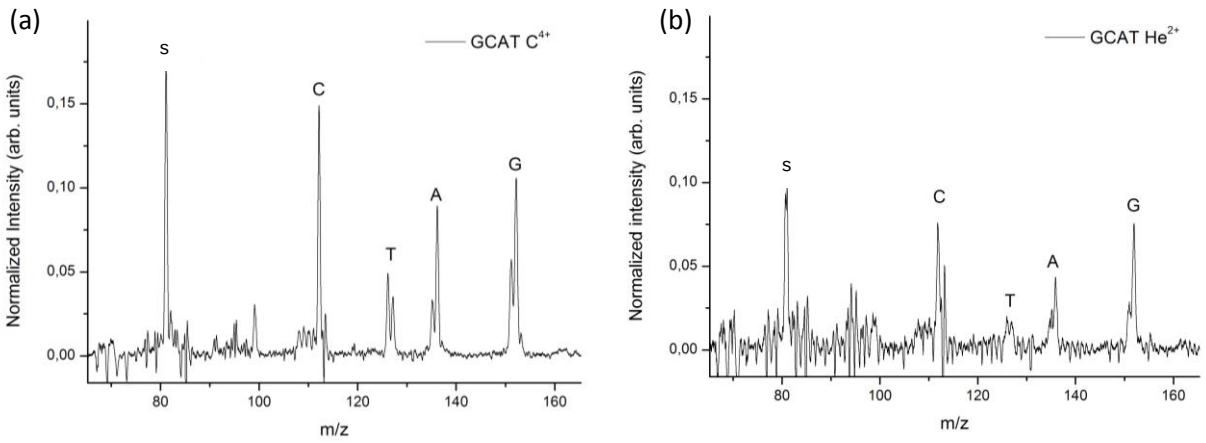

Figure 5.2a and b: The main fragmentation peaks for C^{4+} and He^{2+} irradiation of d(GCAT).

intensity of the thymine peak as compared to the other nucleobases is notable in both cases. This can also be seen in all other d(GCAT) spectra taken with different charge states and ion velocities. To quantify this notion, the "main" peaks in the spectra have been fitted with a Gaussian in OriginPro 8 and the areas underneath them were calculated. The results are displayed as a function of carbon projectile ion velocity in figure 5.3a and as a function of its charge state in figure 5.3b. The projectile-ion velocity yield measurements were done using the same charge state, C^{4+}, and the charge-state yield measurements were performed at the same projectile ion velocity, 0.36515 atomic units (40 keV kinetic energy).

From figure 5.3a, it can be seen that the fragment product yield decreases for all nucleobases as the projectile ion velocity increases. This may be due to the fact that as the ion velocity increases, the interaction time available for ionisation processes to occur decreases. The cytosine yield shows the most radical drop, which can likely be attributed to it being the strongest peak of the four nucleobases. On the other hand, judging from figure 5.3b, there

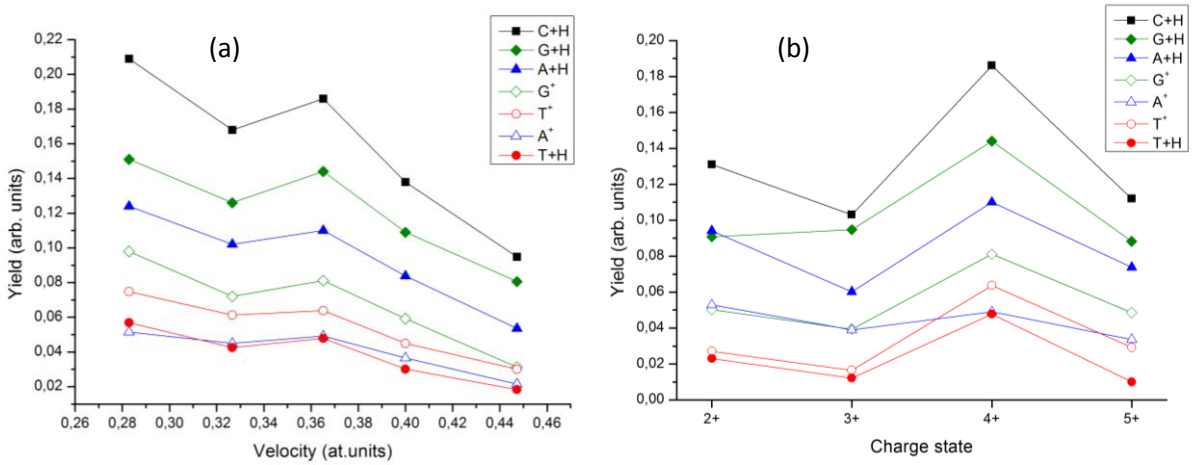

Figure 5.3a and b: Nucleobase-loss yields plotted as function of the C^{4+} projectile ion velocity in atomic units (a), and of projectile ion charge state (b).

appears to be no notable dependence on the ion's charge state. In general, the hierarchy between protonated-nucleobase yields is: C > G > A >> T. Similar calculations were performed with helium as projectile ion. In this case, the yield hierarchy turned out to be G > C > A >> T.

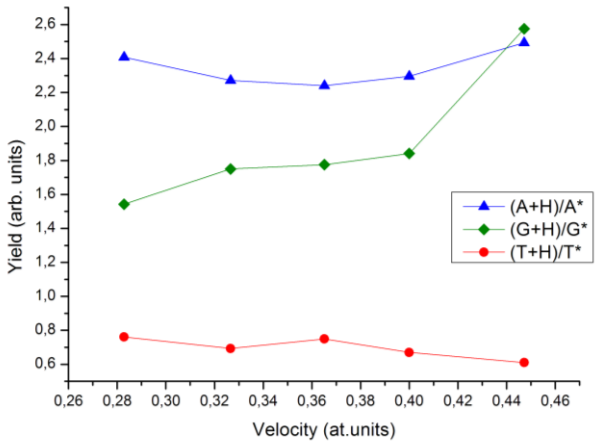

Figure 5.4: Relative changes in protonated/ionised nucleobase yields as a function of projectile ion velocity.

Figure 5.4 was constructed to see how the ratio between the protonated and charged variants of the nucleobases changes. The ratio between protonated thymine and charged thymine decreases slightly. For adenine, not much changes, but for guanine, the balance flips in favour of the protonated variant. In the case of cytosine, only the protonated peak variant was observed in the spectra, hence its absence from figure 5.4. At low ion velocities, i.e. long interaction times, the relative amount of protonated thymine is larger, whereas the relative amount of protonated guanine is less, as compared to shorter interaction times. This notion will become important in section 5.5.

5.2.2 Photonic irradiation

To study the photosensitivity of the molecule, the tetramer was irradiated with photons in the energy range 15 – 570 eV ($\lambda \approx 100 - 2$ nm). At a first glance, the mass spectra for the ionic and photonic irradiation (shown in figure 5.5) look similar. The dominant peaks all correspond

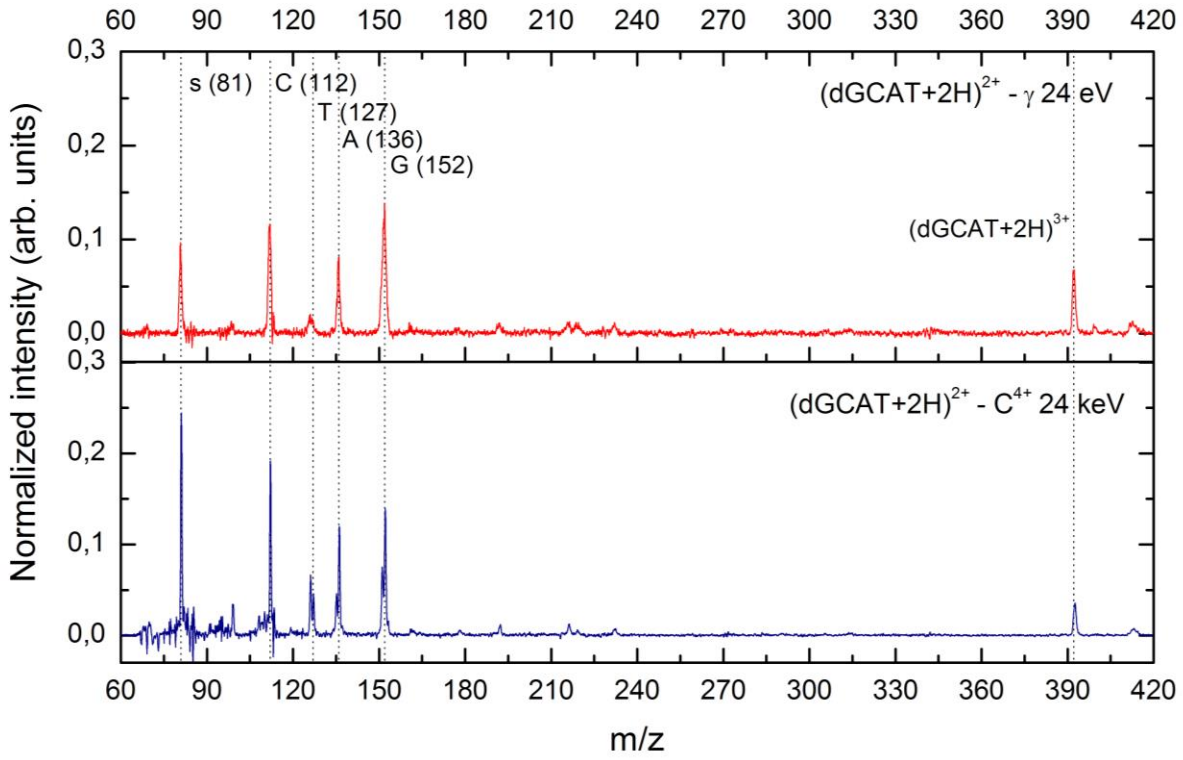

Figure 5.5: Comparing ionic and photonic irradiation of d(GCAT).

to the deoxyribose moiety and the four nucleobases. However, where in the case of ionic irradiation the strongest peak in the spectrum is the one corresponding to the deoxyribose moiety and the nucleobase main contributor is cytosine, the picture looks radically different in the photonic case. The deoxyribose-moiety peak is the third strongest peak, and guanine takes over as most dominant peak. These intensities are however strongly dependent on the photon energy. As was done for the case of ionic irradiation, figures 5.6 and 5.7 display the calculated absolute yields and relative yields, respectively, for the main peaks in the spectrum. These graphs only show the photon energy range 40 – 570 eV, because the lower-photon-energy spectra were taken in a different experiment.

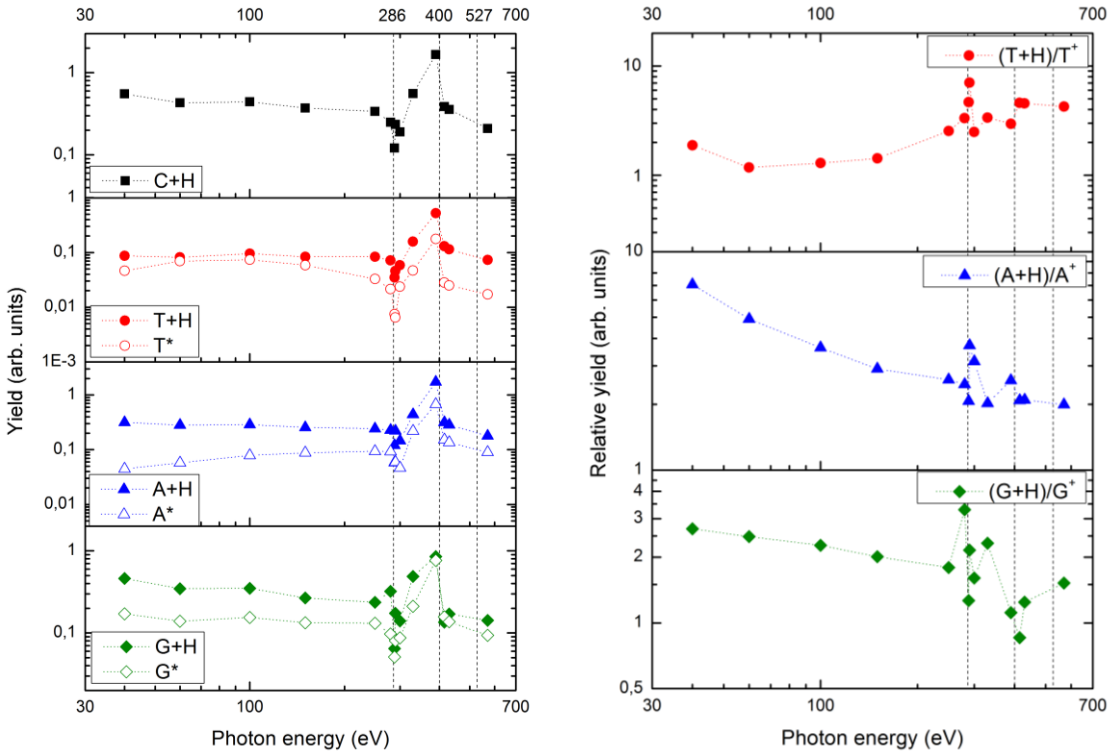

Figure 5.6 and 5.7: Absolute and relative changes in protonated/ionised nucleobase yields as a function of photon energy. The carbon (286 eV), nitrogen (400 eV) and oxygen (527 eV) K-shell edges are indicated by the dashed lines. The dotted connection lines are displayed merely as guide for the eye; they do not show the actual course of the yields. This will be the case for all following figures containing photon irradiation yield data.

The yields show only modest changes when increasing the photon energy, until the carbon, nitrogen and oxygen K-shell edges are reached. At the carbon K-shell edge, the yields drastically decrease for all bases, and at the nitrogen edge, they show a sharp increase. There are not enough data points near the oxygen K-shell edge to see what happens at that energy. When looking at the structure of the oligonucleotide, it can be seen that the nucleobases are the only parts of the molecule that contain nitrogen. The observed rise in yields for nucleobase loss must then be related to this fact. Core shell ionisation of nitrogen can only occur at one of the bases. If the electron hole should transfer to the backbone, it has to pass the bond connecting the base to the backbone, and thereby likely break it. Carbon is present in both the backbone and the nucleobases. There appears to be no reason to expect a drop in the yields here, except for the fact that the geometric cross-section of the backbone is much larger than that of any of the nucleobases. If ionisation at the backbone does not induce base loss, then it would appear that

the backbone acts as a sink for electron holes. This hypothese may be tested by looking at what happens at the phosphorus K-shell edge, since phosphorus is only present in the backbone. If the yields show a large drop at this energy, the hypotheses could be correct.

As for the relative yields, both the relative amount of protonated adenine and guanine decreases with photon energy, but the protonated-thymine yield increases. This is more or less the opposite of what was observed for the ionic case. To get a better view of the changes in nucleobase yields over the different energy regimes, table 5.8 summarizes the results obtained. In all cases, thymine shows the lowest yield. The yields for the VUV photons were obtained from two separate experiments, but the combination of the results of these experiments yields the same hierarchies as when the two experiments are considered separately.

Regime	Charge origin	Yield hierarchy
Ions (q = 2+)	Protonated	G > C > A >> T
	Ionized	G > A > T
Ions (q = 4+)	Protonated	C > G > A >> T
	Ionized	G > T > A
Photons (VUV)	Protonated	C > G > A >> T
	Ionized	G >> A ≳ T
Photons (Soft X-rays)	Protonated	C >> A >> G > T
	Ionized	G > A >> T

Table 5.8: d(GCAT) yield hierarchies for the different scenarios tested. Hierarchies were obtained by calculating the average of nucleobase yields for the given regimes.

An interesting feature is that the hierarchies for the protonated nucleobases for VUV photons and for high charge ions are found to be identical. This can be due to the fact that both types of radiation excite valence band electrons in the tetramer, a feature that will be returned to in section 5.5. For charged-base loss, the hierarchies for both photon energy ranges, as well as the low charge ions are nearly identical. It is also worth noting that the yield for the ionised parent molecule is significantly higher for photonic irradiation (not shown in table 5.8).

The data for the low energy VUV photons was obtained from a different experiment. In this data set, likely due to some technical malfunction at the setup, the peaks for the protonated and charged bases could not be well resolved. As a consequence, only the combined yields for the peak doublets could be determined to an acceptable degree of accuracy. Forcing a double Gaussian through the peaks did give some indication for the separate yields, but, as mentioned before, this did not influence the hierarchies obtained for the VUV photons in table 5.8. Similar to the separate yields in that table, hierarchies for the combined yields are displayed in table 5.9. Again, the hierarchies for the VUV photons and ions match.

Regime	Yield hierarchy
Ions	G > C > A > T
Photons (VUV)	G > C > A >> T
Photons (Soft X-rays)	A > G ≳ C >> T

Table 5.9: d(GCAT) combined yield hierarchies for the different scenarios tested.

5.3 Low on thymine? Just add more!

5.3.1 Effects on ionic irradiation

As mentioned in the previous section, the thymine yield was relatively low with respect to the other nucleobases. An obvious next step is to add thymine to the target molecule to test how this affects the yield. To this end, the main contributor (in the d(GCAT) mass spectra), cytosine, was replaced with thymine, to form the oligonucleotide d(GTAT). A (part of the) resulting mass spectrum is shown in figure 5.11. As would be expected, the thymine yield increases when compared to d(GCAT). However, the yield increase is not so dramatic considering thymine now makes up 50% of the target molecule's nucleobases. This can be seen more quantitatively in figure 5.12a. The yield for protonated thymine is still the lowest, but for charged thymine, the yield now exceeds that of charged adenine and guanine by a

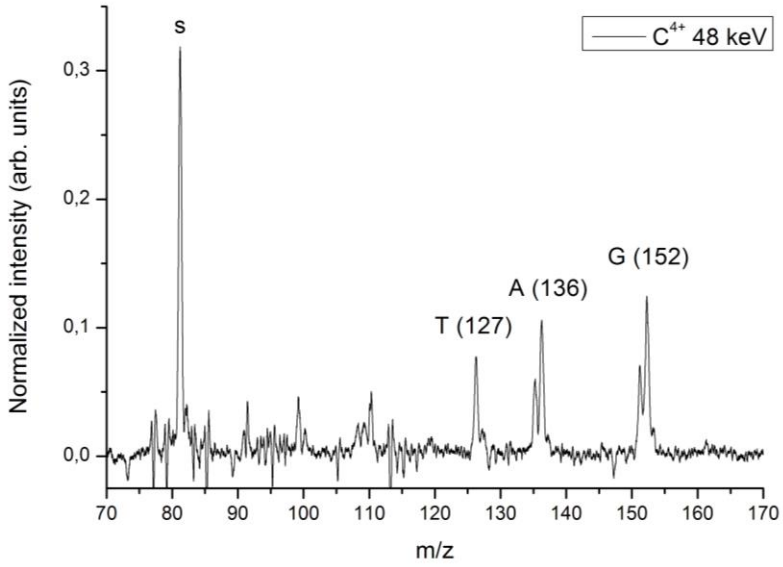

Figure 5.11: Generic mass spectrum for d(GTAT).

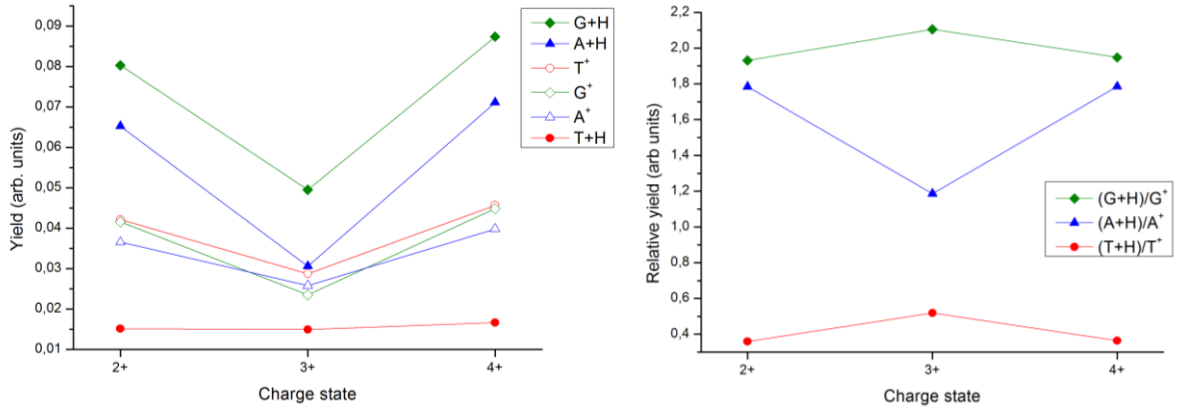

Figure 5.12a and b: Absolute and relative changes in protonated/ionised nucleobase yields as a function of the carbon projectile ion's charge state.

small amount. The nucleobase yields depend in any case only very modestly on the projectile ion charge state. As with d(GCAT), there appears to be a drop at a charge state of 3+. However, no explanation for this particularity could be found. As was done in the case of d(GCAT), the average yields for the nucleobase fragments were calculated, leading to the following hierarchies:

- G >> A >> T *for the protonated nucleobase yields*
- T ≳ G ≳ A *for the charged variants*

As can also be seen from figure 5.12a, figure 5.12b shows that the relative yields between variants are also hardly affected by the change in charge state of the projectile ion.

5.3.2 Effects on photonic irradiation

For photon energies of 40 – 430 eV, the effect of the increased presence of thymine was also studied. Figure 5.13a displays the updated fragment product yields. This time, charged adenine shows the lowest intensity yield, with a notable absence at most tested photon energies. There

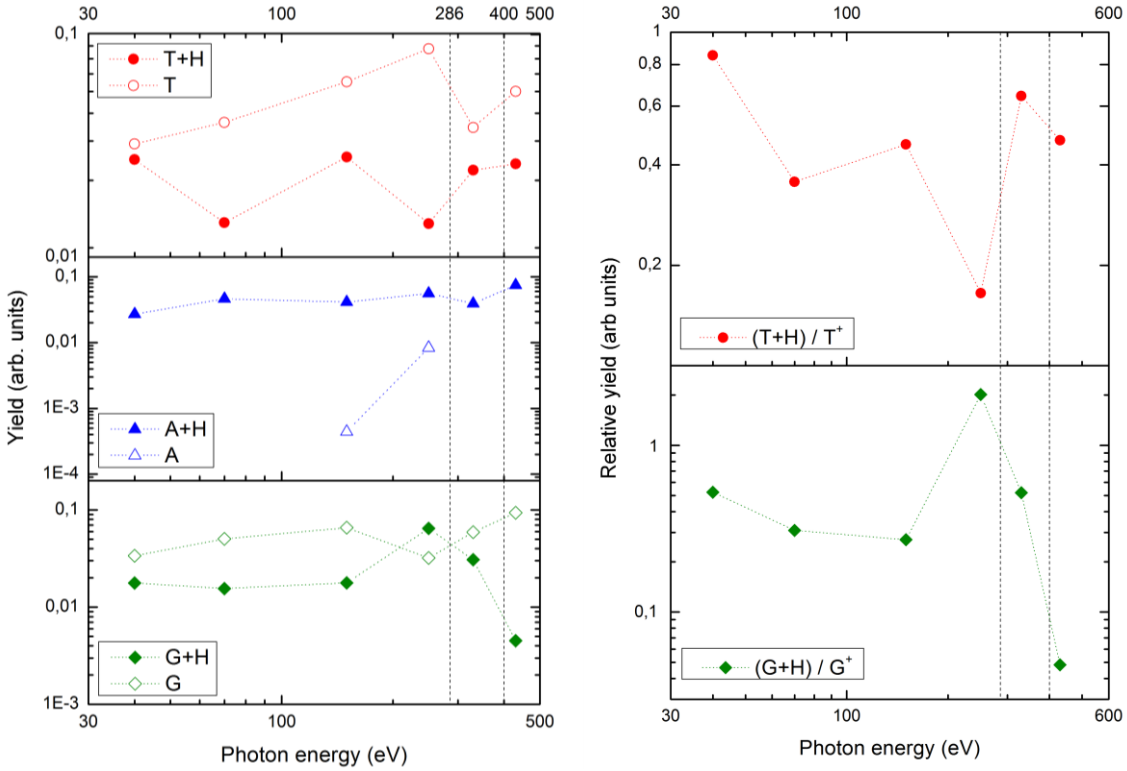

Figure 5.13a and b: Absolute and relative changes in protonated/ionised nucleobase yields as a function of photon energy for d(GTAT). The dashed lines indicate the carbon (286 eV) and nitrogen (400 eV) K-shell edges. The dotted connection lines are displayed merely as guide for the eye; they do not show the actual course of the yields.

appears to be no clear response at the indicated K-shell edges, however, this is likely due to the limited amount of data points in those regions. Analogously to d(GCAT), the following hierarchies can be constructed:

- A >> G > T *for the protonated nucleobase yields*
- G ≳ T >> A *for the charged variants*

Owing to its increased presence in the parent molecule, the charged-thymine yield exceeds that of the one found for d(GCAT). Although the protonated variant still retains its relatively low yield, the yield for the charged version shows a significant increase, rivalling that of guanine. Interestingly, ionised thymine has its maximal yield at a photon energy of 250 eV, whereas guanine has its lowest yield at this energy.

5.4 The weakest link

Returning to figure 5.5, a number of other fragments with relatively lower yields can be identified. Figure 5.14 (next page) shows a calibrated mass spectrum with peak assignments to a number of candidate fragments. Some peaks that only show up at one particular energy are not assigned; only peaks that are common to most spectra are labelled here. Assignments follow that of McCloskey [25].

The fragments at m/z = 192 u, 216 u and 232 u correspond to modified nucleoside loss of cytosine, adenine and guanine, respectively. Formation of these fragments occurs when the 3' C-O phosphodiester bond of the deoxyribose moiety is broken, followed by cleavage at the 5' carbon atom, joining it to the nucleobase (figure 5.15). The fragment with a mass of 192 u, corresponding to modified deoxycytidine loss, was not observed in the d(GTAT) mass spectra, supporting this fragment product assignment. The thymidine fragment is never observed.

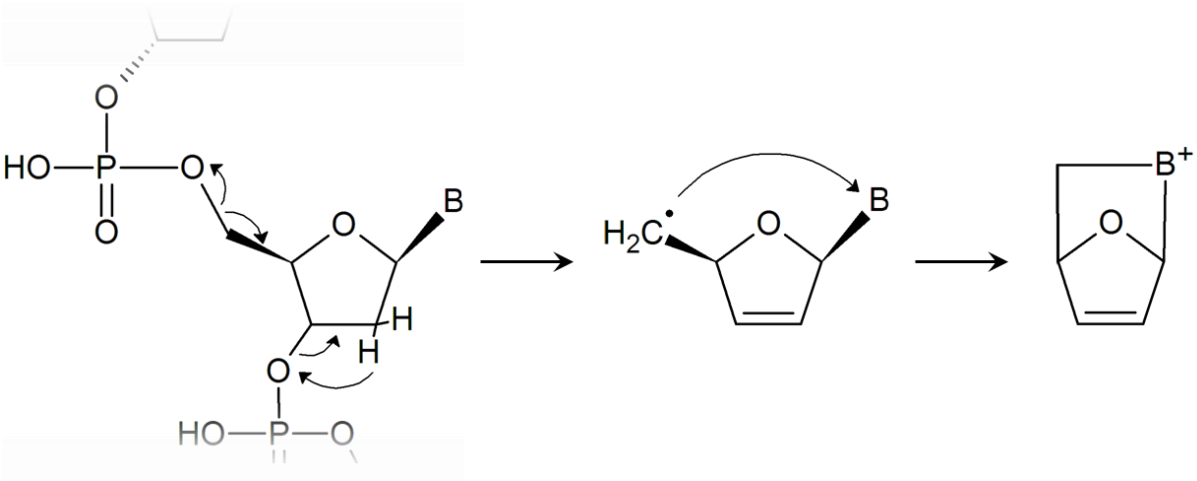

Figure 5.15: Prototype mechanism to create modified nucleoside fragments. Here, B = *cytosine, adenine or guanine to obtain a m/z of* 192 *u,* 216 *u or* 232 *u, respectively.*

In the spectrum shown in figure 5.14, some larger fragments with a m/z exceeding that of the ionised parent molecule can be seen. The fragments at m/z = 412 u and 463 u can be attributed to complementary fragments to nucleoside loss. Cleavage at the 5' carbon atom of dT leads to the formation of the fragment at m/z = 463 u, while dissociation at the same site in dC produces an ion having a m/z of 412 u. The peak of the latter can also be caused by cleavage at the 3' C-O phosphodiester bond of dC and at the 5' carbon atom of dT, leading to the formation of the diphosphate deoxyadenosine ion (pAp). The fragment candidate at m/z = 475 u looks exotic, but involves dissociation of deoxycytidine's sugar moiety by cleavage of its 1' and 4' C – O bonds.

For the low energy photons, a relatively strong peak at m/z = 701 u can be observed. This fragment can be assigned to the parent molecule having lost the nucleosides deoxyguanosine and thymidine or by water abstraction at the 5' terminal, nucleobase loss of adenine and cleavage at the 3' C – O phosphodiester bond of deoxyadenosine.

Lower mass product ions at m/z = 95 u, 99 u and 178 u have been attributed to smaller fragments of the backbone, the structures of which are displayed in figure 5.14.

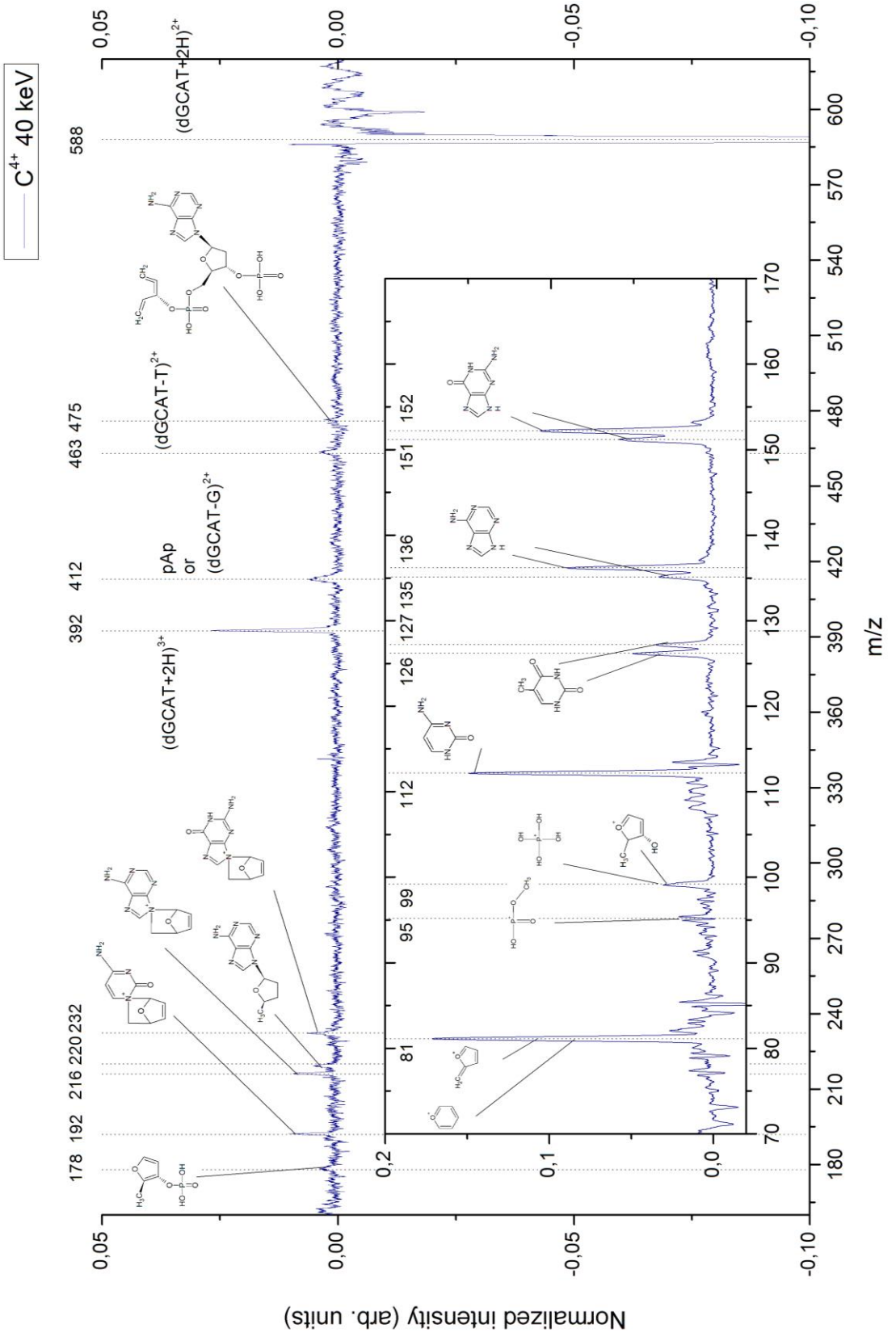

Figure 5.14: d(GCAT) mass spectrum with fragment candidates assigned.

By considering which fragments are produced, and at which intensities they are produced, it is possible to extract information on the 'weak spots' of the molecule, i.e. the bonds that are most likely to break when the molecule is excited. This way, information on how the molecule copes with direct radiation damage can be deduced. Performing the analysis on the spectrum of figure 5.14 reveals that the two weakest bonds by far are the 5' C – O and the 3' C – O phosphodiester bonds of the sugar moiety, with the 5' C – O bond being the weaker of the two. These bonds are comparable to the glycosidic bond strengths, when analysed in a similar fashion. The C – C and P – O bonds appear to be quite stable. As can be deduced from the preceding sections, the outcome of this bond strength analysis is highly dependent on the energy and type of the radiation. Nevertheless, when comparing the different sets of radiation, the 5' and 3' C – O bonds appear to consistently be the weakest link in the backbone. This manifests itself in the readily observed sugar moiety and nucleoside fragments.

Fragments corresponding to the phosphate groups are less frequently observed. It is possible that, owing to their low P_{Ka} [26], these fragments come out as neutrals or negatively charged ions, which cannot be detected using the current configuration.

5.5 Broken bonds and the trends that follow

From figures 5.4 and 5.7, it can be seen that as the interaction time for electron capture decreases, the ratio between protonated and charged nucleobase yields for guanine increases, while that for thymine decreases. Similarly, when increasing the photon energy, this ratio decreases for guanine and adenine, while it increases for thymine. It would appear then that these changes are complementary between guanine and thymine, and that increasing the interaction time for electron capture has a similar effect to increasing the photon energy.

A possible explanation for guanine is that as the photon energy or the interaction time is increased, the base loses its proton due to the higher excitation energy that is being fed into it by the projectile particles. The proton leaves more readily because it is non-covalently bound. This also holds for adenine, but cannot explain the reversed behaviour of thymine, unless the second model in subsection 5.5.2 is correct, since then there is no point to describing this ratio.

The preceding section showed that the bonds that break most easily are the 3' and 5' C – O bonds of the sugar moiety and the C – N bonds joining the nucleobases to the backbone (also called glycosidic bonds). In sections 5.2 and 5.3, yield hierarchies were obtained for the nucleobases. The next part of the discussion proposes explanations for the trends observed for both the nucleobase and deoxyribose moiety yields.

The general path to fragmentation can be described as follows:

1. The target oligonucleotide is ionised.
2. Charge within the molecule is redistributed to lower the total energy.
3. The charge redistribution weakens some of the bonds in the molecule.
4. The excess energy left after the redistribution is sufficient to break to weakened bonds, leading to dissociation.

Which bonds are broken hence depends on the excess energy left after charge redistribution, which in turn depends on the energy transfer process that lead to the ionisation. This is

influenced by the cross sections for e.g. electron capture, auto-ionisation and photo-absorption and the energies of the projectile particles (potential energy in case of the ions and wavelength in case of the photons). A more direct dissociation process, in which the electron that is removed was part of a bond, is also possible.

5.5.1 Nucleobase excision

According to their high intensities in the mass spectra, base loss appears to be a favoured channel. Base loss requires cleavage of the glycosidic bonds in the oligonucleotide molecule, which are highlighted in figure 5.16. Figure 5.17a shows the tetramer zoomed in on one of the nucleobases, guanine. To accomplish base loss, the bond between the 1' carbon of the deoxyribose moiety and the nucleobase needs to be broken. The resulting nucleobase radical will have a mass of 150 u (in the case of guanine). However, no fragment having this m/z is observed (see figure 5.14). A fragment with a mass of 151 u is found, implying that the nucleobase takes with it a proton from the deoxyribose moiety upon cleavage of the bond (shown in figure 5.17b). At a mass of 152 u, an even stronger channel occurs, which has been attributed to the loss of a protonated nucleobase, i.e. the nucleobase carrying an additional, non-covalently bound proton.

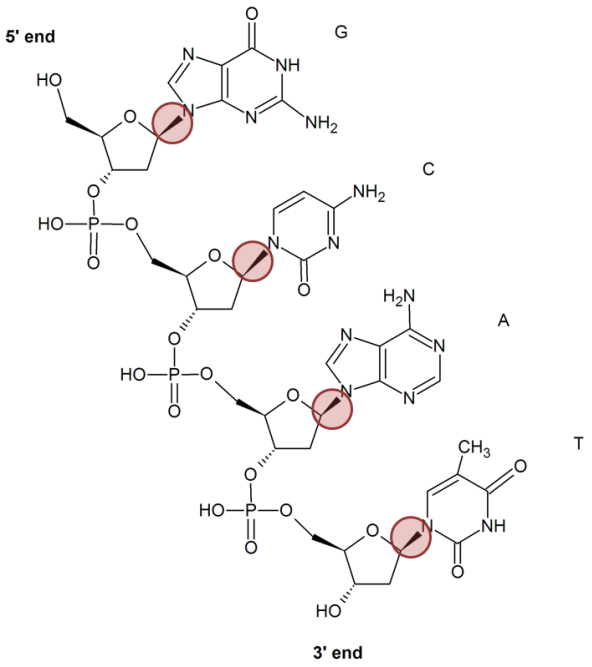

Figure 5.16: The oligodeoxynucleotide d(GCAT) and its glycosidic bonds.

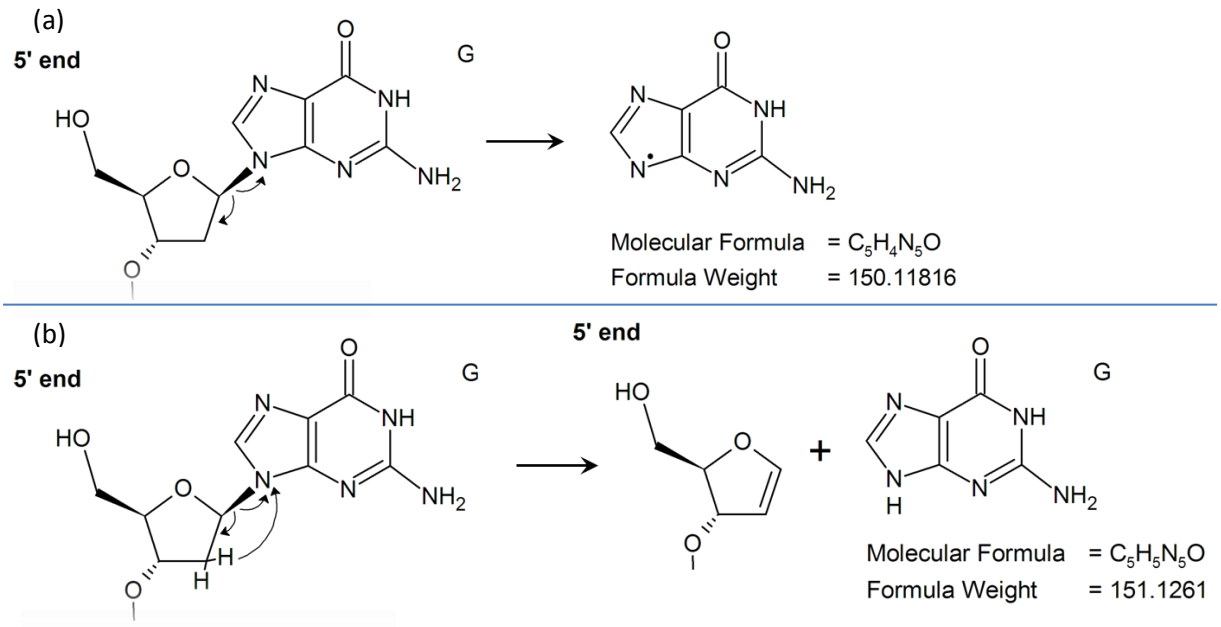

Figure 5.17a and b: The formation of the guanine radical and corresponding neutral, which needs to carry an additional charge in order to be detected. Note: the weights apply to the guanine only.

Recalling that we started out with a doubly protonated oligonucleotide, there would be two protons on the molecule which are not covalently bound, giving them the ability to "move around". These protons are carrying the charge of the molecule. From the fragmentation path mentioned at the beginning of this section, it is evident that the location of these charges plays a key role in the dissociation process of the oligonucleotide. Greco et al. [27] found the proton affinities of the nucleobases to be 9.10 eV for thymine, 9.84 eV for cytosine, 9.76 eV for adenine and 9.90 eV for guanine. The higher the nucleobase proton affinity, the more likely on of the excess protons will be located at (or migrate to) that particular base. Assuming no preferred loss of any of the bases, and with the proton affinities determining which bases will most likely be protonated, this would imply the following hierarchy between protonated-nucleobase yields: G > C > A >> T. In table 5.8, it can be seen that the observed hierarchy differs from this, except for the fact that protonated thymine has a significantly lower yield when compared to the other nucleobases. Even when the parent molecule's nucleobases are composed of thymine for 50% (as it was in d(GTAT)), protonated thymine still comes out having the lowest yield. It therefore seems reasonable to conclude that this can be attributed to its relatively low proton affinity.

Of the regimes listed in table 5.8, only the low charge ions match the predicted hierarchy for protonated-nucleobase loss. However, the proton affinities of guanine and cytosine do not differ much. The proton affinities obviously play an important part in paving the road to fragmentation, but by themselves cannot account for the observed features. Apparently, the incorporation of the nucleobases into a larger molecule requires additional effects to be taken into play.

5.5.2 Models for the nucleobase yields

Experiments performed by Vrkic et al. [15] using classical Collision-Induced Dissociation (many collisions, low energy transfer) showed that the nucleobase yields depend on the nucleobases that are located at the ends of the molecule. They found that base loss occurs preferably at the 5' end of the molecule, except when thymine is located at that end. Base loss at the 3' end was observed to be a suppressed channel. Protonated thymine was hardly ever observed, as is the case in the experiments performed here. Unfortunately, this predicts that guanine should be the strongest peak in the spectra, which in most cases, it isn't.

If Vrkic's results also apply to the charged-base loss, the expectation that guanine should be dominant appears to be supported by table 5.8 and by the results from section 5.3. However, the dominance of charged thymine in the high charge state projectile ion case cannot be explained within this framework.

A more comprehensive model is required then, to explain the apparently preferred base loss of protonated cytosine. It is notable that the nucleobase sequence employed has the same ordering as the proton affinities (G-C-A-T). Doubly protonated, this forms an interesting system. Based on Coulomb repulsion, the protons would preferably be located on the guanine and thymine bases. But the proton affinities would rather have them located on the guanine and cytosine bases instead. The Coulomb repulsion between the freely roaming protons could be responsible for the occurrence of protonated thymine in the spectra, since this channel would be expected to be suppressed.

To try and account for the observed features, two models will now be presented. The first model is based on the following assumptions:

- The molecule is ionised at a random site.
- The electronic redistribution progresses at a finite speed and originates at the ionisation site.
- The proton affinities largely determine where the protons are located.
- Protonation of a base enlarges the probability for base loss. This has been shown by Wan *et al* [28].

Owing to the randomness of the ionisation site, on average, the nucleobases at the centre of the molecule will be exposed to the charge redistribution before the ones at the ends. This can cause the bonds of these bases to break sooner. To quantify this, the leaving group energies for the four bases are 0.11 eV for guanine, 0.17 eV for cytosine, 0.48 eV for adenine and 0.74 eV for thymine [29, 30]. These energies are probably related to the energy it takes in order to remove one of the nucleobases from the oligonucleotide. The energy of the cytosine leaving group is lower than that of adenine, implying that cytosine more readily leaves the parent tetramer. This effect manifests itself in the yield hierarchies as follows:

- Low-energy projectile particles (e.g. low charge state ions), will mostly excite valence band electrons or singly ionise them. Not too much excitation energy is deposited in this case, so the hierarchies will follow the proton affinity ordering: G > C > A >> T.
- High charge state ions and VUV photons always ionise valence band electrons and deposit more excitation energy into the molecule. At this point, the leaving group energies come into play. Since the ionisation site is random by assumption, on average, the bases located in the centre of the molecule will be exposed to the charge redistribution before the ones at the ends. With its lower leaving group energy, cytosine can be able to break its bond before the redistribution has reached guanine at the end. Cytosine base loss will occur more often, leading to the hierarchy: C > G > A >> T.
- X-ray photons ionise core shell electrons and pump more excitation energy into the molecule. In this case, adenine, being in the centre of the molecule, will also be able to break its bond before the redistribution reaches the outer bases. However, since cytosine has the lower leaving group energy, it will still be the first to go, leading to the hierarchy: C > A > G >> T.

All these predictions are consistent with the measured yields in table 5.8. For d(GTAT), simply leaving out the cytosine yields in the predicted hierarchies successfully reproduces the observed ones for this tetramer (see section 5.3).

The second model challenges the peak assignments given in figure 5.14, and that are used throughout the text. It is possible that the peak at m/z = 126 u does not originate from thymine at all. Doubly charged deoxyguanosine and deoxyadenosine both come out having an m/z of 126 u (with cleavages at the appropriate bonds). The current experiment would not be able to distinguish between them. It does however require this relatively small fragment to carry a double charge. One originates from a proton, the other from an electron-hole pair.

From the strength of the bonds that need to be broken to form the fragment (see section 5.4), deoxyguanosine would be more likely to form. If the renewed assignment to the thymine peak were to be true, then this observation can by itself account for the apparent enhanced protonated-nucleobase loss of cytosine. In reality, protonated guanine base loss is the dominant channel as would be predicted by the proton affinities and Vrkic's experiments, but it is

competitive with deoxyguanosine nucleoside loss (both have to form from the same part of the molecule), suggesting that the actual measured yields for protonated guanine come out lower.

A check for this would be to see is the combined yield of deoxyguanosine (which was previously assumed to stem from thymine) and protonated guanine surpasses that of protonated cytosine. This turns out to be the case. Even more, when the photon energy is decreased, the likelihood to form (doubly charged) deoxyguanosine is lower. That would manifest itself in a relative increase in the yield of protonated guanine and an according decrease in the yield of what was assumed to be thymine. At some point, the photon energy is no longer sufficient to remove an additional charge from the already protonated nucleoside, causing this contribution to die out below a certain energy. All these trends are consistent with the data.

If thymine excision is indeed suppressed and the second model is correct, then it would also explain why the thymidine fragment is not observed (section 5.4). Neither of the two models is able to make qualitative statements on the hierarchies for the charged base loss. Table 5.10 suggests that the combined yields largely follow the proton affinities, which could leave a hint towards solving this mystery. It is possible that the small differences in proton affinities between guanine, cytosine and adenine do not manifest themselves in the data at all, in which case none of the models would work.

5.5.3 Strength in numbers

Losing a base can cause the remaining part of the nucleotide to undergo cleavage of the 3' C-O phosphodiester bond of the deoxyribose group. Following proton transfer, further dissociation at the 5' carbon atom yields one (or both) of two isomeric molecules C_5H_5O, as shown in figure 5.18. Although the current experiment is not able to distinguish between any two isomers, according to Sindona and co-workers [31], in oligonucleotide dimers, a six-

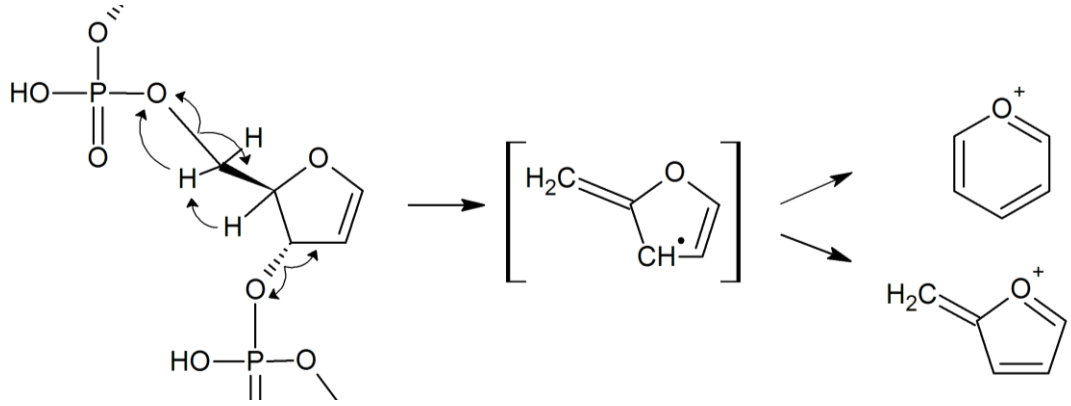

Figure 5.18: The formation of the frequently observed deoxyribose or sugar moiety, having a mass of 81 u. One of two isomers can be formed: the pyranose form (the six-membered ring structure) and the furanose form (the five-membered ring structure).

membered ring intermediate, formed from the deoxyribose moiety, is energetically favourable. Furthermore, Guler *et al.* [32] showed that 2-deoxy-D-ribose tends to exist as a six-membered ring structure in the gas phase (the so-called pyranose form shown in figure 5.18). Bald *et al.* [33] showed that this is also the case in the condensed phase. This would infer that the pyranose form is more likely, although deoxyribose has the furanose form when it is bonded in the oligonucleotide. However, in the current experiment, the fragment product is not the complete deoxyribose molecule (as it was in [32] and [33]), but a portion of it (see also subsection 3.5.3).

The stability of these two molecules may not be comparable. As can be seen in figure 5.14, this fragment, with a mass of about 81 u, is the dominant contributor to most mass spectra. Only at low-energy (< 24 eV) photon irradiation does the contribution decrease, becoming almost negligible below 15 eV photon energies.

The yield calculations were also performed for the deoxyribose moiety, the results of which are displayed in figure 5.19a, b and c. The yield for the ionic irradiation follows the nucleobase yield trend, i.e. it decreases with increasing projectile ion velocity. For the photons, a different trend emerges. In this case, both for d(GCAT) and d(GTAT), the deoxyribose-moiety yield increases with increasing photon energy.

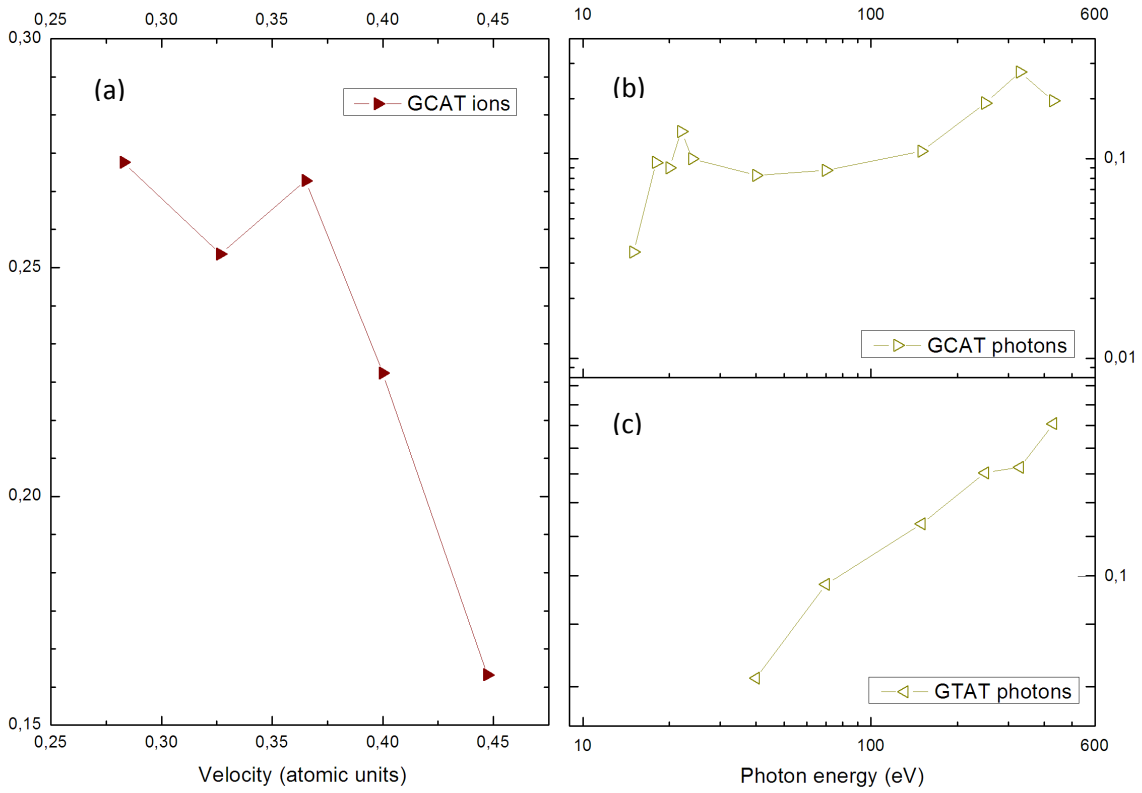

Figure 5.19a, b and c: Yield calculations for the deoxyribose moiety.

Assuming formation of the moiety follows base loss, two more bonds need to be cleaved (see figure 5.18). The higher the photon energy, the greater the probability for this process to occur becomes. Previous experiments had showed the sugar moiety's inability to endure ionisation by electrons [10], photons [11] and keV ions [12, 13]. The reason that it is able to withstand these high energies in this case, is likely due to the fact that the formation process requires cleavage of two (or, actually, three) bonds in the parent oligonucleotide. Dissociation of these bonds carries away sufficient energy for the deoxyribose-moiety molecules to survive. In the case of ionic irradiation, electronic stopping increases linearly with ion velocity. On the other hand, for higher projectile ion velocities, the interaction time for electron capture is lower. This implies that on average, fewer electrons are captured. That means that less energy can be deposited into each molecule, leading to lower fragmentation product formation. Finally, the relative abundance of the moiety in the tetramer likely contributes to the readiness with which it is observed.

Chapter VI
Conclusion

In this chapter, you can find:

- A summary of the results

All truths are easy to understand once they are discovered; the point is to discover them.
- Galileo Galilei

6.1 Putting the pieces together

The effects of different types of ionising radiation on the oligonucleotides d(GCAT) and d(GTAT) has been investigated. Both for ionic and photonic irradiation of the molecules, the deoxyribose nucleotides were found to mostly break apart into their building blocks after being irradiated. Fission into the nucleobases and deoxyribose moieties are observed to be favoured dissociation channels, which also makes sense from a biological point of view; the nucleobases and sugar moiety can readily be reused for synthesizing or repairing other DNA parts.

Most of the observed peaks that showed up in the spectra could be attributed to product fragments of the tetramers. By considering which fragments are produced, and at which intensities they are produced, it was possible to extract information on the 'weak spots' of the molecule, i.e. the bonds that are most likely to break when the molecule is excited. It was deduced that the 5' C – O and the 3' C – O phosphodiester bonds of the sugar moiety and the glycosidic bonds binding the nucleobases to the backbone are the bonds that fission most likely.

For the nucleobases, yield calculations were performed and from this, hierarchies were constructed to see which nucleobases most readily leave the tetramer. These hierarchies have been summarized in table 5.8 and 5.10. In order to reproduce these hierarchies, which don't appear to simply follow the proton affinities as would be expected statistically, two models were presented. The first model was based on the finite progression speed of the charge redistribution following ionisation, the molecule geometry and nucleobase leaving group energy, and the second challenged one of the peak assignments that had been used throughout the text and also in a great deal of other papers on this topic. If the thymine peak would in reality stem from deoxyguanosine, then this could reproduce the hierarchies that have been observed (table 5.8).

A similar effort was made for the deoxyribose moiety yields. Experiments performed on single deoxyribose molecules yielded its total destruction. Although it was found that the C – O bonds of the molecule are some of the weakest bonds in the tetramer, the remaining part was readily observed in the experiment at hand. It was suggested that this is likely due to the fact that the product fragment formation process requires cleavage of three bonds in the parent oligonucleotide. Dissociation of these bonds would carry away sufficient energy for the deoxyribose molecules to survive.

The fragment product yield decreases for all nucleobases as the projectile ion velocity increases. This may be due to the fact that as the ion velocity increases, the interaction time available for ionisation processes to occur decreases. The relative amount of protonated guanine and adenine with respect to their charged variants was found to decrease for both the case of increasing photon energy and increasing interaction time. This could be caused by proton loss as a result of the larger amount of excitation energy deposited in these cases.

Chapter VII
Outlook

In this chapter, you can find:

- A few remarks on the results obtained
- Plans for future improvements
- An outlook for future experiments

I have had my results for a long time: but I do not yet know how I am to arrive at them.
- Karl Friedrich Gauss

7.1 Remarks on the experiments performed

I conclude this story with a few remarks regarding the experiment itself. Regarding the photonic irradiation experiments, there was a clear response at the carbon and nitrogen K-shell edges that have some interesting implications. However, it may have been useful to measure more data points, especially in the vicinity of the oxygen K-shell edge, to better map the resonance that seems to appear when using this photon energy. For the low energy VUV photon experiments, the second buffer gas pulse did not seem to be functioning, resulting in a less than optimal mass resolution. During the next beam time at the BESSY II synchrotron, these measurements are scheduled to be retaken. Also, negatively charged and neutral product fragments could not be observed with the techniques employed in the current setup. As was mentioned in chapter 5, no distinction between any set of isomers could be made in these experiments.

7.2 Outlook

7.2.1 Scheduled experiments and enhancements

One of the enhancements that is being looked into is the possibility to include the so-called negative operation mode for the fragment extraction. By incorporating a very fast high voltage switch into the setup, it should be possible to extract both the positively and the negatively charged product fragments in the same acquisition. This will allow us to detect a more complete spectrum for the molecular fragmentation.

Experiments to extend the oligonucleotide research to include a sequence of special interest for cancer research, the so-called telomere sequence (TTAGGG), are being scheduled to take place at the BESSY II synchrotron facility early 2013. Theory predicts that the telomere sequence is able to trap charges, and thus act as a sink for electron holes created by ionising radiation. In cellular biology, telomeres play an important role in cell division; in particular, they determine when the cell reaches its division limit.

7.2.2 Experiments for model testing

The models described in section 5.5 not only explain the yield hierarchies observed in the mass spectra, but also make some predictions about the outcomes of yield measurements. The first model, based on the finite progression speed of the electronic redistribution following ionisation, the molecule geometry and nucleobase leaving group energy, makes a number of predictions for the outcomes of yield hierarchies for all sequences which can readily be tested.

The second model, which re-assigns the thymine peak to deoxyguanosine, can be tested by measuring the mass spectrum of, for example, d(GGGG), which happens to be scheduled for the near future. If the thymine peak at m /z = 126 u should show up in the mass spectrum of this tetramer, then this would provide strong support for the second model.

Acknowledgements

All of the work described in this document has been performed together with Olmo Gonzalez-Magaña, MSc. I would like to thank Olmo for the pleasant collaboration throughout the past year. I would also like to thank my direct supervisor, dr. Thomas Schlathölter, for all the great suggestions and help. Furthermore, no bag of sweets was safe whenever he was around. I am acknowledgeable to the staff of both the mechanical and electronics workshop at the KVI for their enthusiastic assistance in building and upgrading the setup. And I also extent my thanks to all my colleges here at the Atomic and Molecular Physics group at the KVI for their support and enjoyable company.

References

[1] Mass spectrometry (fragmentation ratios) of DNA base molecules following 80 keV proton impact with separation of direct ionization and electron capture processes; J. Tabet, S. Eden, S. Feil, H. Abdoul-Carime, B. Farizon, M. Farizon, S. Ouaskit, T.D. Märk; *Int J Mass Spectr*, Vol. 292, 53 (2010).

[2] Ion-induced biomolecular radiation damage: from isolated nucleobases to nucleobase clusters; T. Schlathölter, F. Alvarado, S. Bari, A. Lecointre, R. Hoekstra, V. Bernigaud, B. Manil, J. Rangama, and B. Huber; *ChemPhysChem*, Vol. 7 (2006).

[3] Coincidence method for measuring the mass of neutral fragments emitted in a delayed fragmentation process from a singly charged molecule: Fragmentation pathway of adenine; S. Martin, R. Brédy, A.R. Allouche, J. Bernard, A. Salmoun, B. Li, and L. Chen; *Physical Review A*, Vol. 77, 062513 (2008).

[4] Charge driven fragmentation of nucleobases; J. de Vries, R. Hoekstra, R. Morgenstern, and T. Schlathölter; *Physical Review Letters*, Vol. 91, 053401 (2003).

[5] Survival of gas phase amino acids and nucleobases in space radiation conditions; S. Pilling, D. P. P. Andrade, R. B. de Castilho, R. L. Cavasso-Filho, A. F. Lago, L. H. Coutinho, G. G. B. de Souza, H. M. Boechat-Roberty and A. Naves de Brito; *Proceedings IAU Symposium No. IAUS251* (2008).

[6] Photoion mass spectrometry of adenine, thymine and uracil in the 6–22 eV photon energy range; H.-W. Jochims, M. Schwell, H. Baumgärtel, S. Leach; *Chemical Physics*, Vol. 314 p263–282 (2005).

[7] Site-specific dissociation of DNA bases by slow electrons at early stages of irradiation; H. Abdoul-Carime, S. Gohlke, and E. Illenberger; *Physical Review Letters*, Vol. 92, 168103 (2004).

[8] Decomposition of purine nucleobases by very low energy electrons, H. Abdoul-Carime, J. Langer, M.A. Huels, and E. Illenberger; *Eur. Phys. J. D*, Vol. 35, p399–404 (2005).

[9] Collision-induced dissociation of protonated guanine; J. M. Gregson, J. A. McCloskey; *International Journal of Mass Spectrometry and Ion Processes*, Vol. 165/166, p475-485 (1997).

[10] Inelastic electron interaction (attachment/ionization) with deoxyribose; S. Ptasinska, S. Denifl, P. Scheier, and T.D. Märk; *Journal of Chemical Physics*, Vol. 120, p8505-8511 (2004).

[11] Photofragmentation of 2-deoxy-D-ribose molecules in the gas phase; G. Vall-llosera, M.A. Huels, M. Coreno, A. Kivimäki, K. Jakubowska, M. Stankiewicz, and E. Rachlew; *ChemPhysChem*, Vol. 9, p1020-1029 (2008).

[12] Quantification of ion-induced molecular fragmentation of isolated 2-deoxy-D-ribose molecules; F. Alvarado, S. Bari, R. Hoekstra and T. Schlathölter; *Phys. Chem. Chem. Phys*., Vol. 8, p1922–1928 (2006).

[13] Precise determination of 2-deoxy-D-ribose internal energies after keV proton collisions; F. Alvarado, J. Bernard, B. Li, R. Brédy, L. Chen, R. Hoekstra. S. Martin, and T. Schlathölter; *ChemPhysChem*, Vol. 9, p1254 – 1258 (2008).

[14] Collision-induced dissociation of hydrated adenosine monophosphate nucleotide ions: protection of the ion in water nanoclusters; B. Liu, S. Brøndsted Nielsen, P. Hvelplund, H. Zettergren, H. Cederquist, B. Manil and B. A. Huber; *Physical Review Letters*, Vol. 97, 133401 (2006).

[15] Fragmentation reactions of all 64 protonated trimer oligodeoxynucleotides and 16 mixed base tetramer oligodeoxynucleotides via tandem mass spectrometry in an ion trap; A. K. Vrkic, R. A. J. O'Hair, S. Foote, G. E. Reid; *Int J Mass Spectr*, Vol. 194, p145-164 (2000).

[16] A comprehensive study of the low energy collision-induced dissociation of dinucleoside monophosphates; D. R. Phillips and J. A. McCloskey; *International Journal of Mass Spectrometry and Ion Processes*, Vol. 128, p61-82 (1993).

[17] Electronic-vibrational coupling in single-molecule devices; V. Aji, J.E. Moore and C.M. Varma; *arXiv:cond-mat*/0302222v2 (cond-mat.mes-hall) (2003).

[18] Electrospray Ionization for mass spectrometry of large biomolecules; J. B. Fenn, M. Mann, C. K. Meng, S. F. Wong, C. M. Whitehouse; *Science*, Vol. 246, 4926 p64-71 (1989).

[19] Ion funnels for the masses: experiments and simulations with a simplified ion funnel; R. R. Julian, S. R. Mabbett and M. F. Jarrold; *J Am Soc Mass Spectrom*, Vol. 16, p1708-1712 (2005).

[20] *See, for instance*: The influence of peptide structure on fragmentation pathways; S. Bari (PhD Thesis); *Rijksuniversiteit Groningen*, p26-33 (2010).

[21] *See any book on particle accelerators.*

[22] *Website*: MAX-II | MAX-lab, *URL*: https://www.maxlab.lu.se/node/277*, Official website of MAX-lab at the university of Lund, Sweden* (2012).

[23] *Website*: Elektronenspeicherring BESSY, *URL*: http://www.helmholtz-berlin.de/zentrum/grossgeraete/elektronenspeicherring/index_de.html*, Official website of BESSY at the HZB, Germany* (2012).

[24] Characterization of product ions in high energy tandem mass spectrometry of protonated oligonucleotides formed by electrospray ionization; A Weimann , P. Iannitti-Tito and M. M. Sheil; *Int J Mass Spectr*, Vol. 194, p269-288 (2000).

[25] Collision-induced dissociation of polyprotonated oligonucleotides produced by electrospray ionization; J. Ni, M. A. A. Mathews and J. A. McCloskey; *Rapid Com in Mass Spectrom*, Vol. 11, p535-540 (1997).

[26] New aspects of the fragmentation mechanisms of unmodified and methylphosphonate-modified oligonucleotides; S. T. M. Monn and S. Schürch; *J Am Soc Mass Spectrom*, Vol. 18, p984-990 (2007).

[27] Gas-phase proton affinity of deoxyribonucleosides and related nucleobases by fast atom bombardment tandem mass spectrometry; F. Greco, A. Liguori, G. Sindona and N. Uccella; *J Am Chem Soc*, Vol. 112 (25), p9092–9096 (1990).

[28] Fragmentation mechanisms of oligodeoxynucleotides studied by H/D exchange and electrospray ionization tandem mass spectrometry; K. X. Wan, J. Gross, F. Hillenkamp and M. L. Gross; *J Am Soc Mass Spectrom*, Vol. 12, p193-205 (2001).

[29] An ab initio study of tautomerism of uracil, thymine, 5-fluorouracil, and cytosine; M. J. Scanlan and I. H. Hillier; *J Am Chem Soc*, Vol. 106 (13), p3737–3745 (1984).

[30] An investigation of tautomerism in adenine and guanine; M. Sabio, S. Topiol and W. C. Lumma; *J Phys Chem*, Vol. 94 (4), p1366–1372 (1990).

[31] Participation of the nucleobases in the regioselective backbone fragmentation of nucleic acids; A. De Nino, A. Liguori, L. Maiuolo, T. Marino, A. Procopio and G. Sindona; *J Am Soc Mass Spectrom*, Vol. 8, p1257-1261 (1997).

[32] An experimental and computational study of the gas-phase structures of five-carbon monosaccharides; L. P. Guler, Y. Q. Yu and H. I. Kenttämaa; *J. Phys. Chem. A*, Vol. 106 (29), p6754–6764 (2002).

[33] 10–100 eV Ar+ ion induced damage to D-ribose and 2-deoxy-D-ribose molecules in condensed phase; I. Bald, Z. Deng, E. Illenberger and M. A. Huels, *Phys. Chem. Chem. Phys.* , Vol. 8, p1215-1222 (2006).

Appendix A: Mass spectra

In order not to make this document any longer than it already is, the mass spectra will not be shown here, unlike what was promised in section 5.2. Instead, the interested reader may obtain any of the desired spectra by contacting the author.